CZECH TECHNICAL UNIVERSITY IN PRAGUE

Faculty of Electrical Engineering

BACHELOR'S THESIS

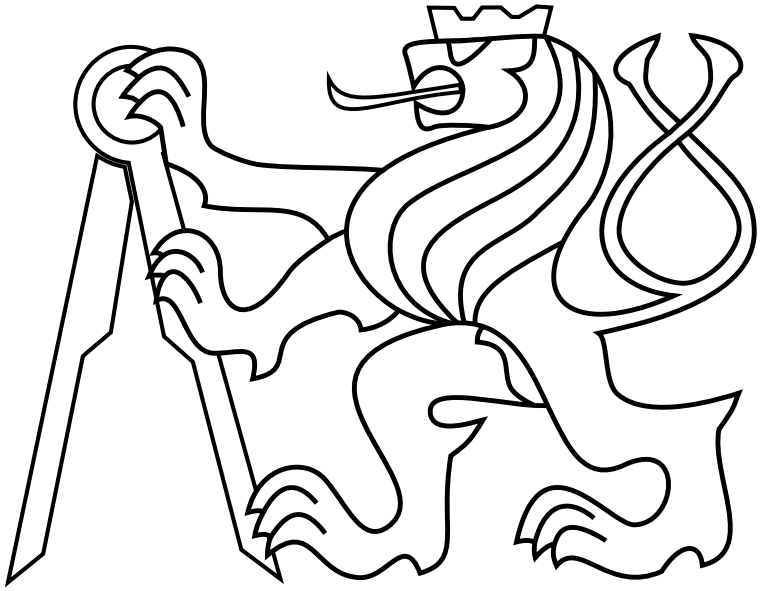

Jakub Konrád

Analysis of Scaling in Distributed Control

Department of Cybernetics

Thesis supervisor: **Ing. Ivo Herman**

Prohlášení autora práce

Prohlašuji, že jsem předloženou práci vypracoval samostatně a že jsem uvedl veškeré použité informační zdroje v souladu s Metodickým pokynem o dodržování etických principů při přípravě vysokoškolských závěrečných prací.

V Praze dne .....

.....
Podpis autora práce

Acknowledgements

Firstly, I would like to thank my supervisor Ing. Ivo Herman for his patience, guidence and advice. Additionally, I would like to thank my family for their constant support during my study.

Abstract

The goal of the thesis to study the effects of random disturbances on various distributed control systems and to prepare and run simulations required to do so. The simulations focus mainly on the overall behavior of the systems subjected to random disturbances as well as the scaling of the output variances of these systems. Thesis verifies and compares scaling in distributed systems with optimal and suboptimal localized control. The effect of various communication structures as well as the influence of static nonlinearities is assessed.

Key Words: distributed control, vehicle platoons, scaling, optimal control, static nonlinearities

Abstrakt

Cílem práce je studovat efekty náhodného šumu na různé systémy s distribuovaným řízením a připravit a provést k tomu potřebné simulace. Simulace jsou zaměřeny hlavně na celkové chování systémů vystavených náhodnému šumu a na škálování rozptylu výstupů těchto systémů. Práce ověřuje a porovnává škálování u systémů distribuovaného řízení s optimálními a neoptimálními regulátory. Dále je ověřován vliv různých struktur komunikačního grafu, statických nelinearit a okrajových podmínek.

Klíčová slova: distribuované řízení, kolony vozidel, škálování, optimální řízení, statické nelinearity

Czech Technical University in Prague
Faculty of Electrical Engineering

Department of Cybernetics

BACHELOR PROJECT ASSIGNMENT

Student: Jakub K o n r á d

Study programme: Cybernetics and Robotics

Specialisation: Robotics

Title of Bachelor Project: Analysis of Scaling in Distributed Control

Guidelines:

1. Study the results in the field of coherence and optimal control of distributed systems.
2. Prepare simulations for verification of scaling in distributed systems with optimal localized control.
3. Assess the effects of static nonlinearities, boundary conditions and communication graph structure.
4. Implement local Model Predictive Control and verify the performance and scaling of the overall system.

Bibliography/Sources:

[1] B. Bamieh, M. R. Jovanović, P. Mitra, and S. Patterson, “Coherence in Large-Scale Networks: Dimension-Dependent Limitations of Local Feedback,” Autom. Control. IEEE Trans., vol. 57, no. 9, pp. 2235–2249, 2012.
[2] K. Hengster-Movric and F. Lewis, “Cooperative Optimal Control for Multi-agent Systems on Directed Graph Topologies,” Autom. Control. IEEE Trans., vol. 56, no. 3, pp.769-774, Mar.2014.
[3] F. L. Lewis, H. Zhang, K. Hengster-Movric, and A. Das, Cooperative Control of Multi-Agent Systems, Springer, p. 307, 2014.
[4] W. B. Dunbar and D. S. Caveney, “Distributed Receding Horizon Control of Vehicle Platoons: Stability and String Stability,” IEEE Trans. Automat. Contr., vol. 57, no. 3, pp. 620–633, Mar. 2012.

Bachelor Project Supervisor: Ing. Ivo Herman

Valid until: the end of the summer semester of academic year 2015/2016

L.S.

doc. Dr. Ing. Jan Kybic
Head of Department

prof. Ing. Pavel Ripka, CSc.
Dean

Prague, January 23, 2015

České vysoké učení technické v Praze
Fakulta elektrotechnická

Katedra kybernetiky

ZADÁNÍ BAKALÁŘSKÉ PRÁCE

Student: Jakub K o n r á d

Studijní program: Kybernetika a robotika (bakalářský)

Obor: Robotika

Název tématu: Analýza škálování v distribuovaném řízení

Pokyny pro vypracování:

1. Seznamte se s výsledky v oblasti koherence a optimálního řízení distribuovaných systémů.
2. Připravte simulace pro ověření škálování optimálních regulátorů v distribuovaném řízení.
3. Ověřte vliv statických nelinearit, okrajových podmínek a struktury komunikačního grafu.
4. Vyzkoušejte vliv lokálního prediktivního řízení (MPC) pro jednotlivé agenty na celkové chování systému.

Seznam odborné literatury:

[1] B. Bamieh, M. R. Jovanović, P. Mitra, and S. Patterson, “Coherence in Large-Scale Networks: Dimension-Dependent Limitations of Local Feedback,” Autom. Control. IEEE Trans., vol. 57, no. 9, pp. 2235–2249, 2012.
[2] K. Hengster-Movric and F. Lewis, “Cooperative Optimal Control for Multi-agent Systems on Directed Graph Topologies,” Autom. Control. IEEE Trans., vol. 59, no.3, pp.769-774, Mar.2014.
[3] F. L. Lewis, H. Zhang, K. Hengster-Movric, and A. Das, Cooperative Control of Multi-Agent Systems, Springer, p. 307, 2014.
[4] W. B. Dunbar and D. S. Caveney, “Distributed Receding Horizon Control of Vehicle Platoons: Stability and String Stability,” IEEE Trans. Automat. Contr., vol. 57, no. 3, pp. 620–633, Mar. 2012.

Vedoucí bakalářské práce: Ing. Ivo Herman

Platnost zadání: do konce letního semestru 2015/2016

L.S.

doc. Dr. Ing. Jan Kybic
vedoucí katedry

prof. Ing. Pavel Ripka, CSc.
děkan

V Praze dne 23. 1. 2015

Contents

List of Figures

1 Introduction

The control of the vehicle platoons has been a popular field of study in recent decades. Besides the extensive theoretical research on the subject, there are several projects utilizing the findings in practice. Among these projects are California Partners for Advanced Transportation Technology (PATH), a research and development program of the University of California, Berkeley focused on Intelligent Transportation Systems research, founded in 1986 [13], or the Safe Road Trains for the Environment (SARTRE) project, funded by the European Commission under the Framework 7 programme, whose goal is to develop strategies and technologies to allow vehicle platoons to operate on normal public highways [1].

One of the results of the studies is that in order to achieve satisfactory results, it is necessary to broadcast some global information, ie. state of the leader, to the whole formation [2].

According to [2], if all vehicles of the communication network are exposed to random disturbances, it is not possible to maintain a large coherent formation using only localized feedback.

If we achieve the best localized feedback, the behavior of the formation is reasonable on "microscopic" level. That is, distances between vehicles and their velocity are maintained. However, if the formation is inspected as a whole, we can observe slow, long spatial wavelength modes. The formation then exhibits an "accordion-like" motion going through the whole formation [2].

The goal of this thesis is firstly to prepare and run simulations that replicate the results in [2]. Secondly, to test the behavior of the systems with optimal control, systems with static nonlinearities and other types of systems subjected to random disturbances and compare these results to results in [2].

Thesis is divided into four main chapters. First chapter studies the effect of random disturbances on linear systems with localized feedback. Second chapter is focused on system with localized optimal control. Third chapter examines the behavior of selected systems from the first chapter with added static nonlinearities and finally, fourth chapter takes the simulations from previous chapters and runs them on second order system with PI controller.

Note that the fourth chapter was originally supposed to be focused on systems with the model predictive control. However, after an agreement with the supervisor of the thesis it was decided to change the topic of the chapter.

As previously mentioned the simulation-focused parts examine results published in [2].

The theoretical parts of the project mainly draw from works targeted on distributed control and vehicle platoons [9, 2, 4, 8].

2 Linear systems localized control

This chapter examines behavior of large-scale interconnected systems, with communication structure similar to vehicular formations, subjected to random disturbances [2]. Ideally, the vehicles match each others velocity and positioning with constant spacing.

2.1 System descriptions

Before we describe the formation and structure of the systems, we need to define the subsystem representing one vehicle. The vehicle is represented by double integrator with state space control. We define two states for each vehicle, its position and velocity. We can describe the system by equations (1) and (3).

$$\dot{x_i} = v_i \tag{1}$$

$$\dot{v_i} = k_p((x_{i-1} - x_i + \Delta) - (x_i - x_{i+1} + \Delta)) + k_v((v_{i-1} - v_i) - (v_i - v_{i+1})) \tag{2}$$

$$= k_p(x_{i-1} - 2x_i + x_{i+1}) + k_v(v_{i-1} - 2v_i + v_{i+1}). \tag{3}$$

where x_i represents position of i-th vehicle, v_i velocity of i-th vehicle, k_p position feedback gain and k_v velocity feedback gain. The goal is to control the system so that intervals between vehicle positions remain constant. Position of adjacted vehicles is compared and the result is weighed by position feedback gain. In ideal case the actual position difference $d_i = x_{i-1} - x_i$ is equal to desired spacing with interval Δ. As for velocity, the aim is for all vehicles in the platoon to have the same velocity, so that the difference $v_{i-1} - v_i$ equals zero.

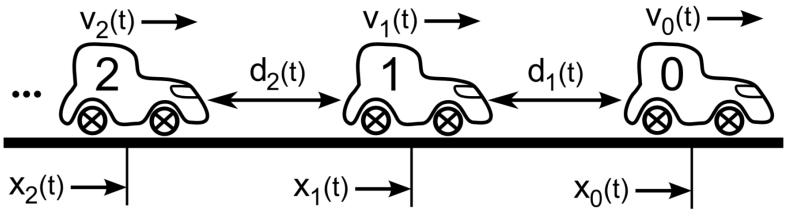

Figure 1: Platoon of vehicles with leader [11].

Figure 1 represents the platoon of vehicles with leader. It is one of the communication structures we describe later in this chapter. States of each vehicle are illustrated in the picture as well as the distances between adjacted vehicles.

The state space model:

$$\dot{\mathbf{x}} = A\mathbf{x} + B\mathbf{u} \tag{4}$$

$$\dot{\mathbf{y}} = C\mathbf{x} \tag{5}$$

for state vector $\mathbf{x}$, inputs $\mathbf{u}$ and outputs $\mathbf{y}$ we get matrices A, B, C, D:

$$A = \begin{pmatrix} 0 & 1 \\ 0 & 0 \end{pmatrix} \qquad B = \begin{pmatrix} 0 \\ 1 \end{pmatrix} \tag{6}$$

$$C = \begin{pmatrix} k_p & k_v \end{pmatrix} \qquad D = \begin{pmatrix} 0 \end{pmatrix} \tag{7}$$

As for the values of k_p and k_v, in this chapter they were chosen empirically as $k_p = 1$ and $k_v = 1$. This chapter focuses on reproducing the results presented in [2] on various types of systems. While creating a state space controller using one of control theory metods might change some behaviour of the system (ie. amplitude of the oscilations) it should not affect quality of the results. This is examined more in following chapter where we simulate systems with optimal state space control.

Subsystems are linked together to create required communication structure.

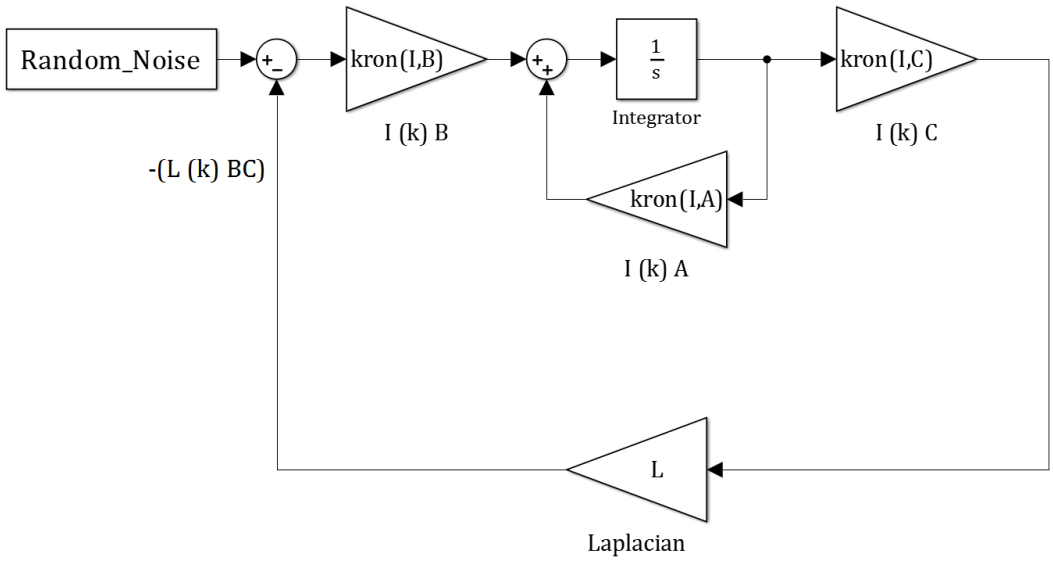

Figure 2: Block representation of the created system

Regardless of chosen structure, final system can be described by following equation (see figure 2)

$$\dot{x} = (I_N \otimes A - L \otimes BC)x \tag{8}$$

where communication structure of the system is described by the graph Laplacian L. [9]

2.1.1 Graph theory basics

Before we explain meaning of the graph Laplacian, we need to present some basic graph theory concepts. A Graph is a pair $G = (V, E)$ with $V = \{v_1, ..., v_N\}$ being a set of N nodes

and E a set of edges. Elements of E are denoted as (v_i, v_j) which is termed an edge from v_i to v_j and represented as an arrow with tail in v_i and head in v_j. In-degree of v_i is a number of edges having v_i as a head. For our purposes, we can represent the communication structure of the system as communication graph. In that case vehicles are represented as nodes in the graph and communication between two vehicles is depicted by edges [9].

2.1.2 Laplacian matrix

Laplacian matrix (Laplacian) is a matrix representation of the communication graph. If we define in-degree matrix $D = diag(d_i)$ and adjacency matrix $A = [a_{ij}]$ with weights $a_{ij} > 0 \; if \; (v_i, v_j) \in E$, where E is the set of edges of the communication graph. Then we define Laplacian matrix as $L = D - A$. The properties of the graph and therefore the system can be studied in terms of its Laplacian. The Laplacian matrix is of extreme importance in the study of dynamic multi-agent systems [9].

2.1.3 Kronecker product

Kronecker product ($\otimes$) is an operation on two matrices with following definition:
Let us have two matrices $A = [a_{ij}]$, B, we define the kronecker product $A \otimes B$ as $A \otimes B = [a_{ij}B]$, where $[a_{ij}B]$ is a matrix with block elements $a_{ij}B$ [6]. The example of Kronecker product for two matrices:

$$M1 = \begin{pmatrix} 2 & 1 \\ 0 & 3 \end{pmatrix} \qquad M2 = \begin{pmatrix} 1 & 3 \\ 2 & 6 \end{pmatrix} \qquad M1 \otimes M2 = \begin{pmatrix} 2 & 6 & 1 & 3 \\ 4 & 12 & 2 & 6 \\ 0 & 0 & 3 & 9 \\ 0 & 0 & 6 & 18 \end{pmatrix}$$

2.1.4 1-D torus

1-D Torus [2] is the simplest of communication structures studied in this thesis. It represents 1-D cyclical structure, where each vehicle recieves information only from the adjacent vehicles.

All models of vehicles in this network are equal and each one communicates only with two neighboring vehicles.

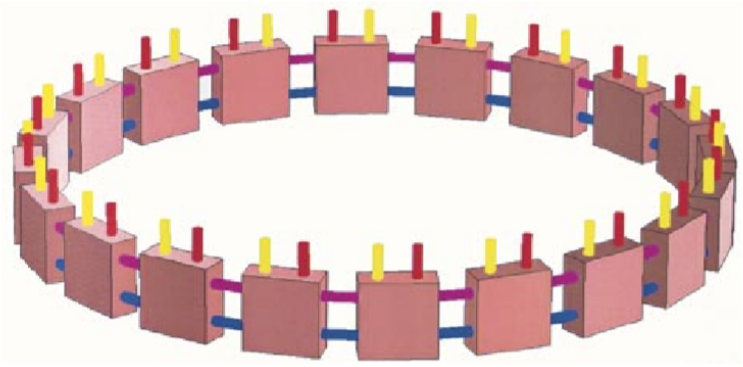

Figure 3: Picture of 1-D toroidal communication structure [3].

Because of this, we obtain symmetrical Laplace matrix with twos on main diagonal (9).

$$L_4 = \begin{pmatrix} 2 & -1 & 0 & -1 \\ -1 & 2 & -1 & 0 \\ 0 & -1 & 2 & -1 \\ -1 & 0 & -1 & 2 \end{pmatrix} \tag{9}$$

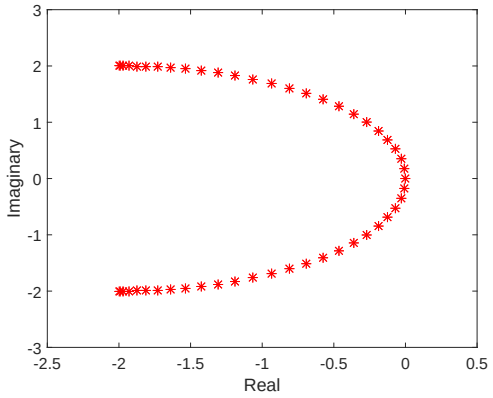

Figure 4: Eigenvalues of 1-D torus

Graph in the figure 4 displays eigenvalues of 1-D torus system created according to (8). We can observe that all eigenvalues are situated in left half-plane of the complex plane. This ensures the stability of the system.

2.1.5 2-D and 3-D torus

These systems are multidimensional analogies of the 1-D torus. It means that each vehicle draws information from 2d other vehicles adjacent to it in the communication graph, where d is dimension of the network.

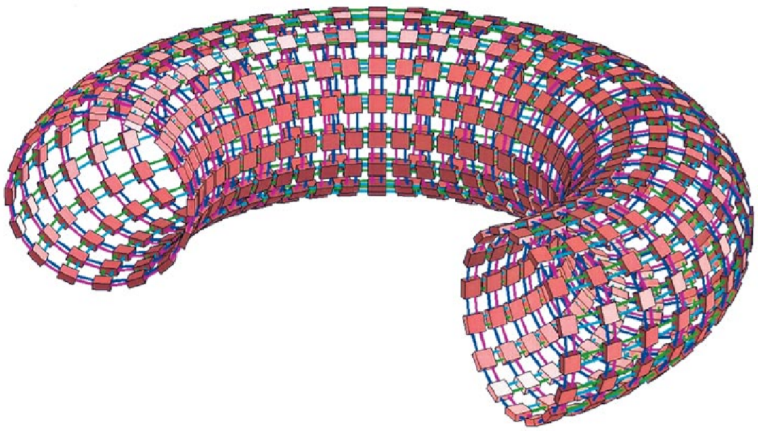

Figure 5: Picture of 2-D toroidal communication structure [3].

It is important to note that while these vehicles are adjoining in the communication structure, they are not necessarily next to each other in the physical platoon. The Laplacian is a representation of the communication structure of the platoon. This structure however can be completely different than platoon's physical layout. Laplace matrix for this type of structure is symmetrical, with 2d on the main diagonal. Example of the Laplacian for 2-D torus consisting of 9 vehicles (10).

$$L_{3\times 3} = \begin{pmatrix} 4 & -1 & -1 & -1 & 0 & 0 & -1 & 0 & 0 \\ -1 & 4 & -1 & 0 & -1 & 0 & 0 & -1 & 0 \\ -1 & -1 & 4 & 0 & 0 & -1 & 0 & 0 & -1 \\ -1 & 0 & 0 & 4 & -1 & -1 & -1 & 0 & 0 \\ 0 & -1 & 0 & -1 & 4 & -1 & 0 & -1 & 0 \\ 0 & 0 & -1 & -1 & -1 & 4 & 0 & 0 & -1 \\ -1 & 0 & 0 & -1 & 0 & 0 & 4 & -1 & -1 \\ 0 & -1 & 0 & 0 & -1 & 0 & -1 & 4 & -1 \\ 0 & 0 & -1 & 0 & 0 & -1 & -1 & -1 & 4 \end{pmatrix} \tag{10}$$

2.1.6 1-D leader-follower

In previously described systems all vehicles were equal. In leader-follower structure, there is a vehicle called leader, in our case the first vehicle, that is not controlled by feedback from the other vehicles. The leader drives independently of the platoon and acts as a referential agent. Other vehicles of the system - the followers work the same way as in 1-D torus system, with the exception of the last follower. The last vehicle of the platoon communicates only with the previous follower and is not connected to the leader.

$$\dot{x_N} = v_N \tag{11}$$

$$\dot{v_N} = k_p(x_{N-1} - x_N + \Delta) + k_v(v_{N-1} - v_N). \tag{12}$$

As a result, the communication graph is not circular as it was in case of 1-D torus. This fact is evident when we look at Laplacian for this type of structure. Also note that in this case

Laplacian is no longer symmetric because of the zeros in the first row representing the leader (13).

$$L_4 = \begin{pmatrix} 0 & 0 & 0 & 0 \\ -1 & 2 & -1 & 0 \\ 0 & -1 & 2 & -1 \\ 0 & 0 & -1 & 1 \end{pmatrix} \tag{13}$$

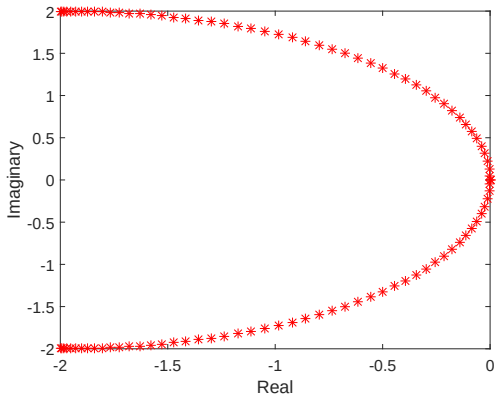

Figure 6: Eigenvalues of 1-D leader-follower structure

Graph in the figure 6 displays eigenvalues of 1-D leader-follower structure. Similarly to torus, eigenvalues of leader-follower structure also lie in the left half-plane of the complex plane, ensuring the stability of the system.

2.1.7 1-D leader-follower with asymmetric control

The leader-follower structure with asymmetric control is a variant of a leader-follower structure from previous section. Followers in both structures draw feedback from the adjacent vehicles. In system with symmetric control, the feedback gain in both directions, towards the leader and away from it, is the same. This is not the case for asymmetric control. In system with asymmetric control feedback gain in one direction is stronger. Here we can see two types of asymmetric control: control with stronger gain towards the leader (forward) and control with stronger gain in direction opposite than the leader's (backward). In this thesis we will only simulate system with forward asymmetric control because the transient period for systems with backward asymmetric control is too long for the purpose of our simulations. For example for system of 100 vehicles with bacward control it can take up to 10^5 seconds before the last car moves at speed comparable to that of the leader [12].

The equation (14) shows an example of Laplacian of the leader-follower structure with

forward asymmetric control (forward gain $g_{fw} = 1$, backward gain $g_{fw} = 0.5$)

$$L_4 = \begin{pmatrix} 0 & 0 & 0 & 0 \\ -1 & 1.5 & -0.5 & 0 \\ 0 & -1 & 1.5 & -0.5 \\ 0 & 0 & -1 & 1 \end{pmatrix} \tag{14}$$

2.2 Vehicle trajectory simulation

All vehicles are subjected to random disturbances. We study vehicle position trajectories relative to vehicle number one both on "macroscopic" and "microscopic" scale [2].

Firstly, we created model of the desired system according to (8). The creation of the system in Matlab enviroment is fairly straightforward. The only problem is the creation of the laplace matrix for desired system. Scripts used to create laplace matrix for 1-D system were provided by supervisor of the project Ivo Herman. In simulations of 2-D a 3-D structures we utilized script [7].

For the purposes of this simulation we created systems of 50 vehicles (64 for 2-D and 3-D torus). Random disturbances were created by function $randn()$, which generates normally distributed random numbers. For toroidal structures the random disturbances variance was set to $Var = 0.11$, for leader-follower structures the variance was set to $Var = 0.01$. The required distance between vehicles was set to $\Delta = 1$. The initial conditions for starting positions were set to match desired spacing of the platoon and initial velocities were set to zero.

2.2.1 Results of the simulation

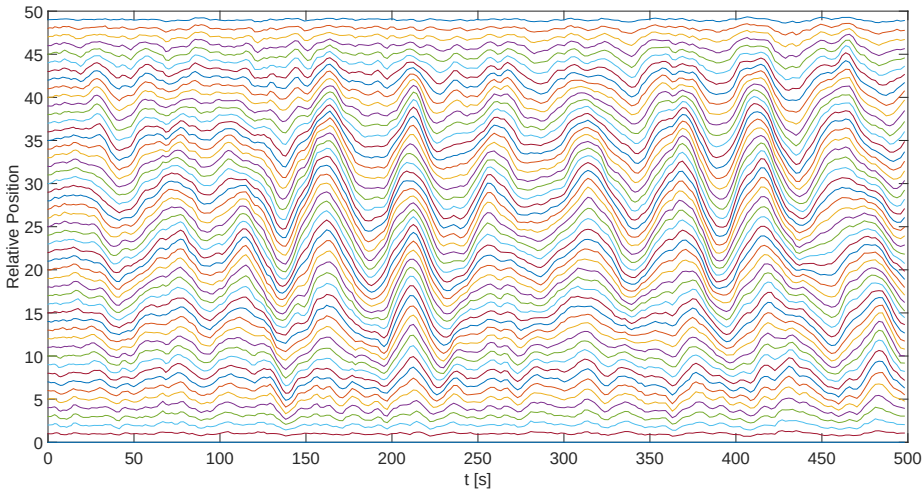

Figure 7: Vehicle position trajectories of a 50 vehicle 1-D toroidal communication structure.

The figure 7 displays vehicle position trajectories of a 50 vehicle 1-D toroidal communication structure. The vehicles in the middle of the graph, that is positions 15 to 35, are the furthest in the communication structure from the vehicle nubmer 1 used as reference for position. Here we can observe the strongest accordion-like motion in the formation.

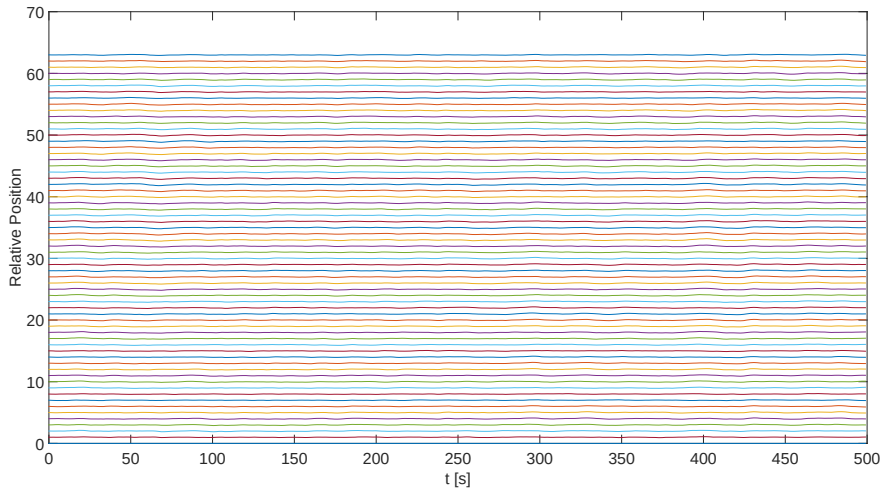

Figure 8: Vehicle position trajectories of a 64 (8x8) vehicle 2-D toroidal communication structure.

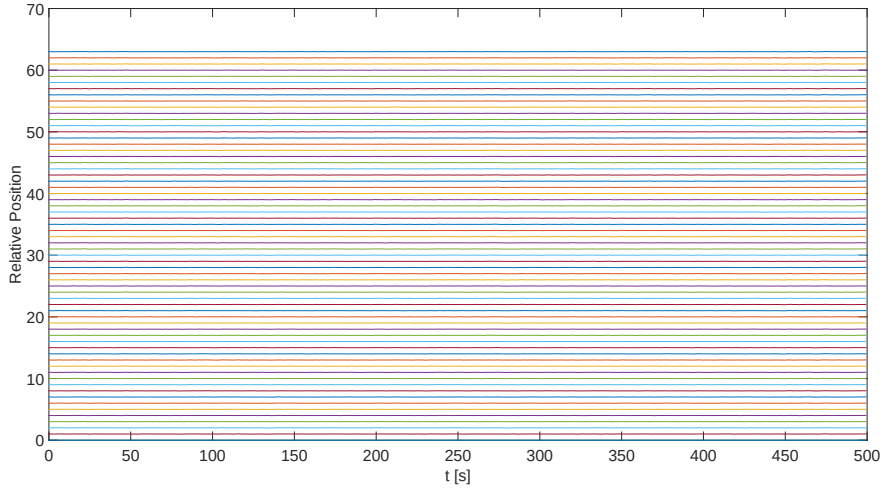

Figure 9: Vehicle position trajectories of a 64 (4x4x4) vehicle 3-D toroidal communication structure.

As we can see in figures 8 and 9, 2-D and 3-D communication structures are more robust than previously examined 1-D structure. It is clear that 2-D and 3-D structures are much less volatile when exposed to random disturbances. The accordion-like motion is not observable. We need to take into consideration that graph radius of 2-D and 3-D structures is much

smaller than radius of 1-D structures with comparable number of vehicles. Unfortunately due to insufficient computing capacity we were not able to run the simulations for 2-D and 3-D structures with equivalent graph radius.

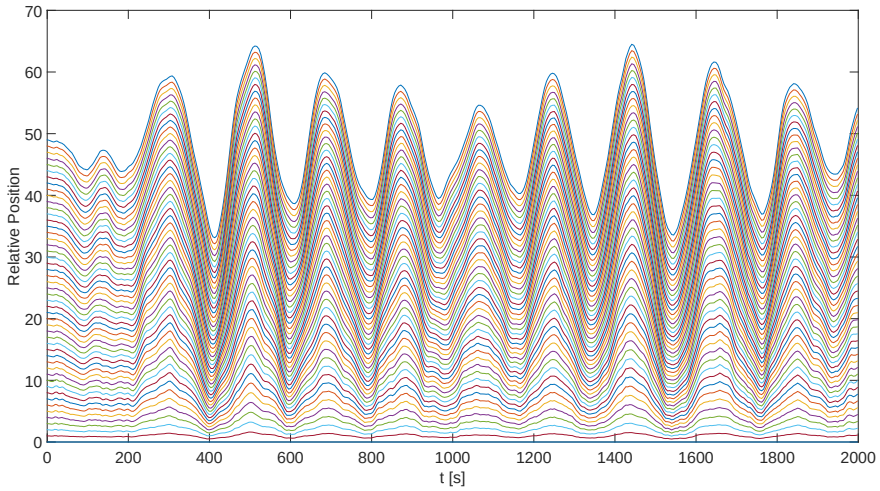

Figure 10: Vehicle position trajectories of a 50 vehicle 1-D leader-follower communication structure.

In figure 10 are the results of simulation with 50 vehicle 1-D leader-follower communication structure. In contrast to the previous structures, the leader follower structure is not circular but linear. It means maximum distance between two vehicles is N and not N/2. As a result of this, despite the lower variance of random disturbances (0.01 instead of 0.11 for torus), the accordion-like motion in the system is more pronounced.

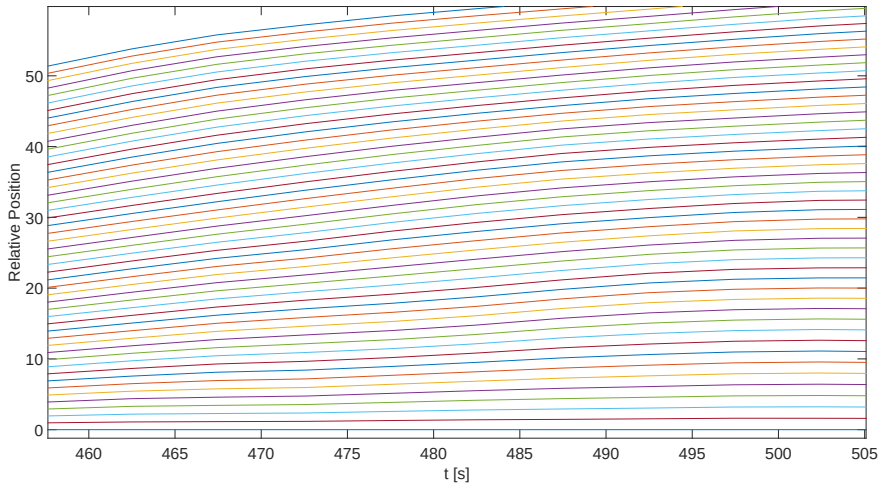

Figure 11: Figure is a zoomed in version of the graph in figure 10. The graph is showing the well regulated distances between vehicles.

The figure 11 shows a "zoomed in" version of the graph in figure 10. Here we can see that despite the sizable slow oscillation of the entire system, vehicle to vehicle distances in the platoon are stable and well regulated.

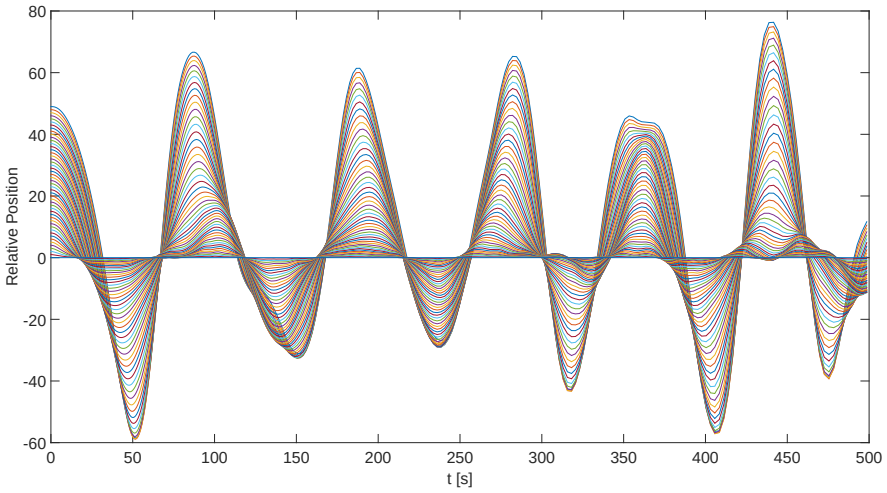

Figure 12: Vehicle position trajectories of a 50 vehicle 1-D leader-follower communication structure with forward asymmetric control.

Figure 12 displays results of the simulation for system with forward asymmetric control with forward gain $g_{fw} = 1$ and backward gain $g_{bw} = 0.9$. The graph shows an accordion-like oscillation similar to that in figure 10. For asymmetric control however, there is an overshoot, where the last vehicles of the platoon cross the position of the leader. This more volatile behavior is caused by the fact that feedback between vehicles in the direction of the leader is stronger than feedback in the opposite direction [5].

2.3 Performance measures

In following subchapters we will focus on scaling of various performance measures with system size for previously described systems. Please note that performance measures described in this subchapter are the same as the performance measures defined in [2]. Some of these measures can be considered steady state variances of outputs of linear systems [2]. Let us have a linear system

$$\dot{x} = Ax + Bu$$
$$y = Cx.$$

In all examined cases outputs y of the system have finite variances. That means the output has a finite steady state variance V, which is quantified by the square of the H_2 norm of the system [2]:

$$V := \sum_{k \in N} \lim_{t \to \infty} E\{y_k^*(t) y_k(t)\} \tag{15}$$

where k ranges over all vehicles N of the system and y_k is the output of the k-th vehicle. Symbol * represents complex conjugate transpose and E is expected value.

We then define the individual output variance [2] as

$$E\{y_k^* y_k\} := \frac{1}{N} \sum_{l \in N} \lim_{t \to \infty} E\{y_l^*(t) y_l(t)\} \; = \; \frac{V}{N} \tag{16}$$

Below we describe three performance measures: local error, deviation from average and disorder. Local error is considered microscopic measure because it describes local variables associated with any given state. Disorder and deviation from average are considered macroscopic measures as they involve quantities associated with whole network or nodes that are far apart in the network [2].

2.3.1 Local error

Local error measures the difference between neighboring vehicles. When inspecting vehicular formations, local error is the difference $\tilde{x}_k$ of actual positions of the neighbooring vehicles from their proper spacing [2].

$$y_k := \tilde{x}_k - \tilde{x}_{k-1} \text{ [2]} \tag{17}$$

2.3.2 Deviation from average

Deviation from average corresponds with the difference between each vehicle's position error and average of these errors [2].

$$y_k := \tilde{x}_k - \frac{1}{N} \sum_{l \in N} \tilde{x}_l \text{ [2]} \tag{18}$$

2.3.3 Long range deviation (disorder)

Long range deviation matches the error of the distance between the two most distant vehicles from what it should be. If we were to look for the most distant vehicle from vehicle k it would be the vehicle with index $k + \frac{N}{2}$. Then the distance between these vehicles would be $\Delta \frac{N}{2}$ where Δ is desired distance between two vehicles [2].

$$y_k := x_k - x_{k+\frac{N}{2}} - \Delta \frac{N}{2} = \tilde{x}_k - \tilde{x}_{k+\frac{N}{2}} \text{ [2].} \tag{19}$$

The description above is only true for systems with 1-D toroidal communication structure. It is possible to expand the definition for multidimensional systems [2]. However, it has proven difficult to define disorder for systems with leader-follower structure. We have decided to use disorder as defined in (19) for all types of tested systems. Due to this the performance measure

refered to as disorder in this thesis is different from disorder described in [2] for all studied communication structures with the exception of 1-D torus.

Despite mentioned difference, disorder used in this thesis still meets the requirements to be considered macroscopic performance measure and therefore all findings concerning macroscopic measures should still apply.

2.4 H_2 norm and Lyapunov equation

Previous subchapter mentions that we can quantify variances of our performance measures as H_2 norm squared of the system. We compute H_2 norm as:

$$\|G\|_2 = \sqrt{\int_{-\infty}^{-\infty} trace[g^*(t)g(t)]\, dt} \text{ [14]} \tag{20}$$

where $g(t)$ is the impulse response. Moreover, we can write

$$\|G\|_2^2 = trace[B^*QB] = trace[CPC^*] \tag{21}$$

where Q and P are observability and controllability Gramians. To obtain the Gramians we solve following Lyapunov equations for P and Q [14]:

$$AP + PA^* + BB^* = 0 \qquad A^*Q + QA + C^*C = 0 \tag{22}$$

2.5 Performance measures simulation

The simulation aplying previously described performance measures consists of two separate parts. Firstly, we took systems created for vehicle trajectory simulations, altered their output matrices (C) so that they correspond with output described in the performance measures subchapter and tried to compute their H_2 norm squared by solving Lyapunov equations. Secondly, we tried to compute the steady state variance of the system outputs from simulations described in chapter 2.2.

2.5.1 Variance using Laypunov equation

To solve Lyapunov equations (22) matlab function *lyap*() was used. This function is part of Control System Toolbox. First, we tried to solve Lyapunov equation for Q to get the observability gramian, from which variance can be easily computed using trace [2]. This has proven to be unsuccessful due to the fact that the equation could not be solved by *lyap*() function for our systems. We tried using the same approach for controllability gramian. This way it was possible to compute variances for 1-D and 2-D torus. To compute variance for 3-D torus, we were forced to use different feedback gain $k_p = 1.1,\ k_v = 1$ to successfully solve Lyapunov equation. Note that the feedback gain $k_p = 1.1,\ k_v = 1$ was only utilized in performance measure simulation for 3-D torus, all other simulations in this chapter use feedback gain $k_p = 1,\ k_v = 1$ as stated previously.

The described problem with solving Lyapunov equation however presisted for systems with leader. Due to this we were not able to compute variances for these systems using Lyapunov equation and compare them to variances obtained by simulation described below.

2.5.2 Variance using vehicle trajectory simulation

To compute variances by simulation, the vehicle trajectory simulation described in chapter 2.2 was used. Here the variance of random disturbances was set to $Var = 1$ for all communication structures. According to [2] the system outputs have finite steady state variance. To obtain it we run the vehicle trajectory simulation for chosen number of iterations (in this case 300) and computed the variance for selected times. After a period of time the result settled on the output variance for selected performance measure.

2.5.3 Results of the simulation

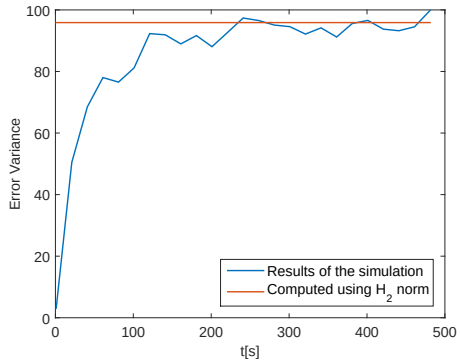

(a) Local error

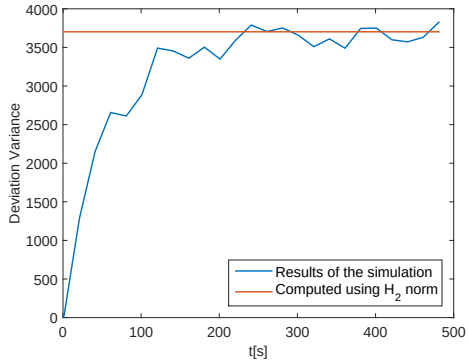

(b) Deviation from average

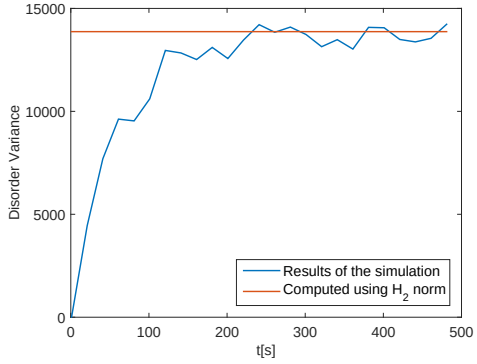

(c) Disorder

Figure 13: Comparison between values of performance measure variances obtained via simulation and variances computed from H_2 norm for 1-D torus.

In figure 13 we can see the results of our simulation compared to variance computed using H_2 norm. Figure 13 shows variance of 1-D torus structure of 48 vehicles. From the graph it is clear that after certain period of time (here approximately after 250 seconds) variance obtained from vehicle trajectory simulation settles on the same value that we gained by computing H_2 norm squared of the system. This was the case not only for the 1-D toroidal structure but for all other structures the simulation was performed on.

This is an expected result consistent with the theory provided above as well as the findings published in [2].

For the results of this simulation for other communication structures please see appendix B. Note that the simulations and the results can be found on attached CD.

2.6 Scaling verification

According to [2], upper bounds of performance measures individual output variances for toroidal structures asymptotically scale in terms of vehicle quantity N and number of dimensions of the comunication network d. We assume that these two factors are the only ones that affect the type of the scaling. Following this line of thought all tested 1-D systems should fall to the same category.

The table 1 below describes different scaling of d-dimensional systems of N vehicles for both microscopic (local error) and macroscopic (disorder and deviation from average) performance measures.

	Microscopic	Macroscopic
$d = 1$	N	N^3
$d = 2$	$log(N)$	N
$d = 3$	1	$N^{1/3}$

Table 1: Scaling of different communication structures [2]

To verify this we run the vehicle trajectory simulation, previously used to compute performance measure individual output variances (16) for our communication structures, with various numbers of vehicles, plotted the results and compared them to expected scalings according to table 1. As we can see in the table 1, all macroscopic measures should scale the same way. Scaling of both deviation from average and disorder was only included for 1-D torus. For scaling of disorder variance for other communication structures please see appendix C or attached CD.

2.6.1 Results of the simulation

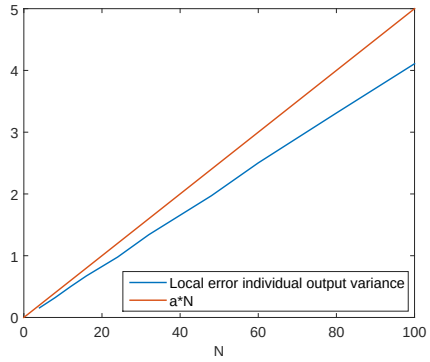

(a) linear axes

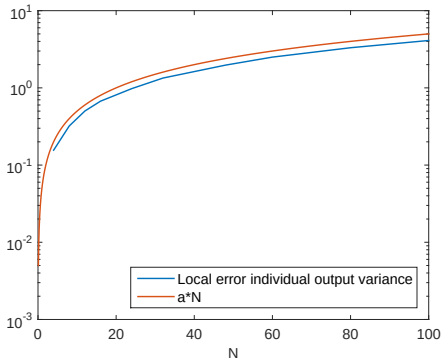

(b) semilog axes

Figure 14: Scaling of local error individual output variance for 1-D torus.

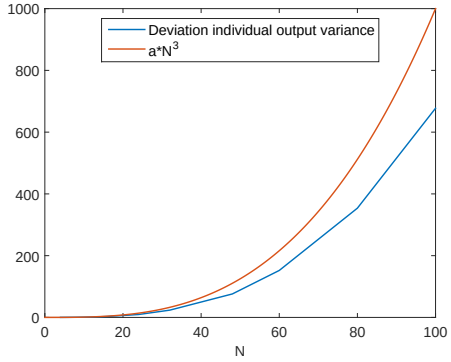

(a) linear axes

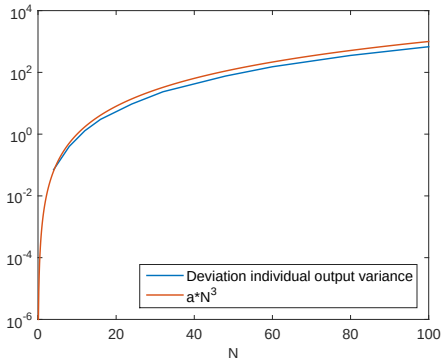

(b) semilog axes

Figure 15: Scaling of deviation from average individual output variance for 1-D torus.

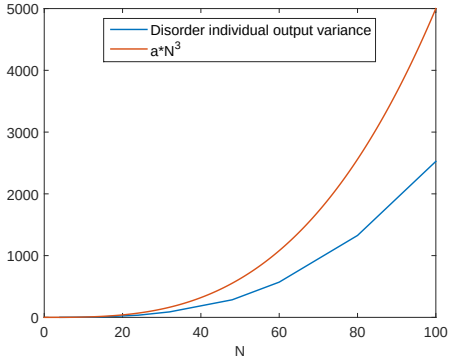

(a) linear axes

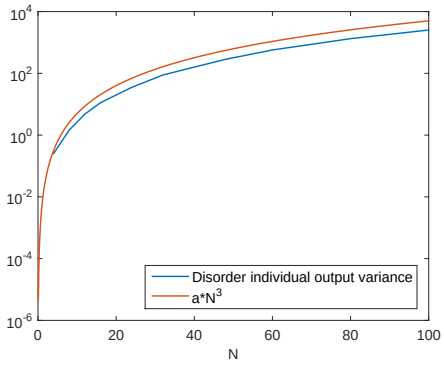

(b) semilog axes

Figure 16: Scaling of disorder individual output variance for 1-D torus.

Graphs in figures 14, 15 and 16 show the scaling of performance measure variances for 1-D torus. The results of the simulations are in each graph compared to corresponding function to illustrate expected scaling. Note that the added mathematical functions are only supposed to represent the type of scaling (linear, cubic) and scaling rate itself is not supposed to be the same (that is, for example variance of local error can scale linearly but with lower slope than added linear function).

Graphs on the left depict the variance in linear axes. For more convinient comparison of the scaling, graphs on the right have logarithmic y axes. In semi-logarithmic axes we can see, that both curves are of the same shape and are only vertically displaced. This means that depicted functions differ only in coefficient and not qualitatively.

Graphs in figure 14 show scaling of local error for 1-D torus. The scaling of local error variance is clearly linear, which is consistent with table 1.

Graphs in figures 15 and 16 represent the scaling of macroscopic performance measures, that is deviation from average and disorder. The type of scaling in both figures is consistent with added cubic function. This also corresponds with table 1.

Since it is clear that the type of scaling for deviation from average and disorder is the same, from this point forward we will only include figures showing scaling of deviation variance. As for the simulations showing scaling of disorder variance, results for this chapter are included in the appendix C. Results of the simulations for this and all following chapters are viewable on attached CD.

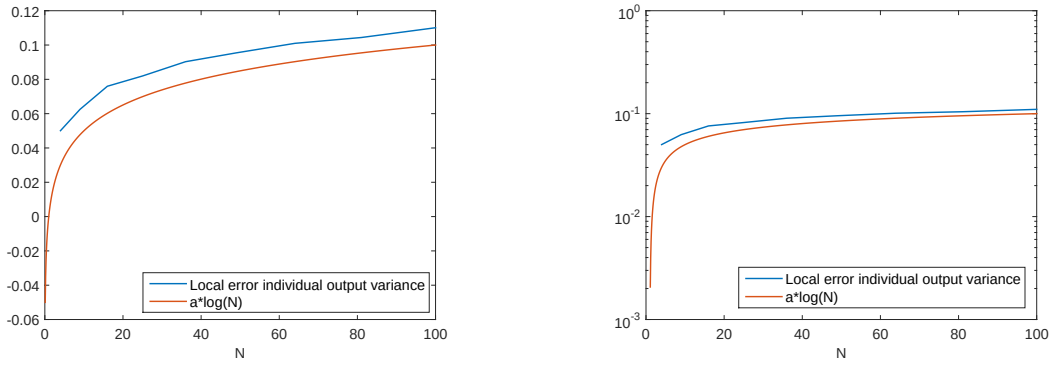

(a) linear axes

(b) semilog axes

Figure 17: Scaling of local error individual output variance for 2-D torus.

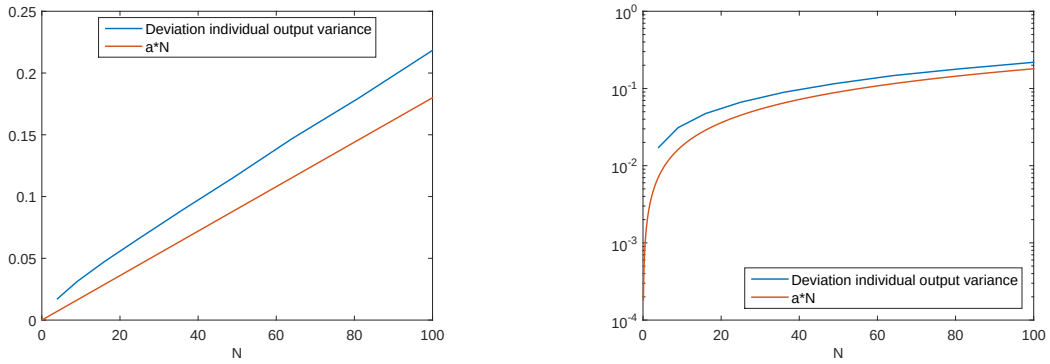

(a) linear axes (b) semilog axes

Figure 18: Scaling of deviation from average individual output variance for 2-D torus.

Graphs in figure 17 depict the scaling of local error variance for 2-D toroidal communication structure. According to the table 1 the scaling for 2-D structure is logaritmical. In the graph we can see that the results of the simulation follow displayed logaritmical function.

The scaling of macroscopic measure variance for 2-D structure is supposed to be linear. Figure 18 shows that this is clearly the case.

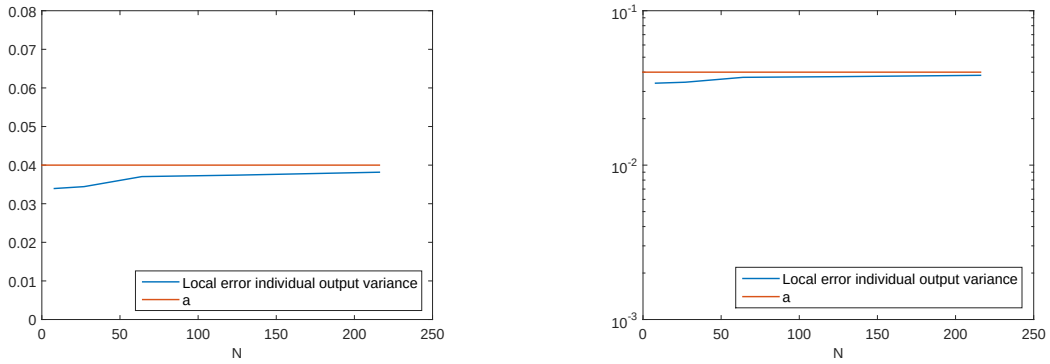

(a) linear axes (b) semilog axes

Figure 19: Scaling of local error individual output variance for 3-D torus.

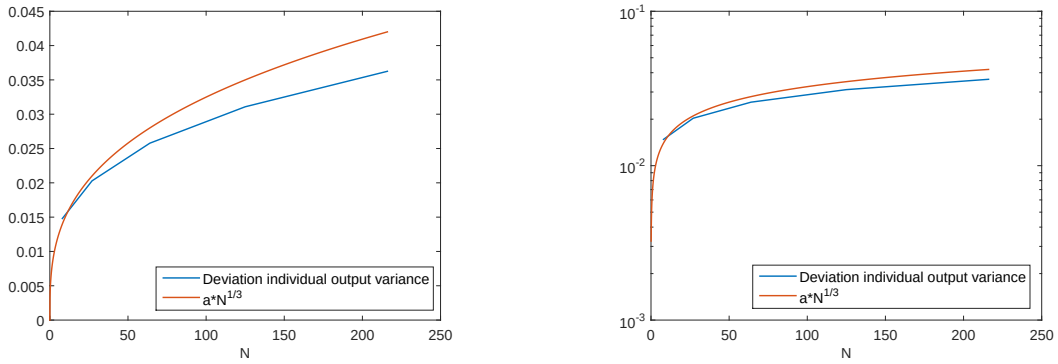

(a) linear axes (b) semilog axes

Figure 20: Scaling of deviation from average individual output variance for 3-D torus.

Results of the simulation for 3-D torus are shown in figures 19 and 20. For 3-D communication structure microscopic scaling should be constant. Macroscopically the system should scale with $aN^{1/3}$. From mentioned graphs it is clear that variances scale appropriately.

During the course of the simulations for 1-D leader-follower structures, we discovered that the simulation time needed for performance measure variances to settle for leader-follower structures is many times longer than for toroidal structures with comparable vehicle count (figure 21). As mentioned in 2.5.1, for these systems we were also not able to confirm the performance measure variances using Lyapunov equation.

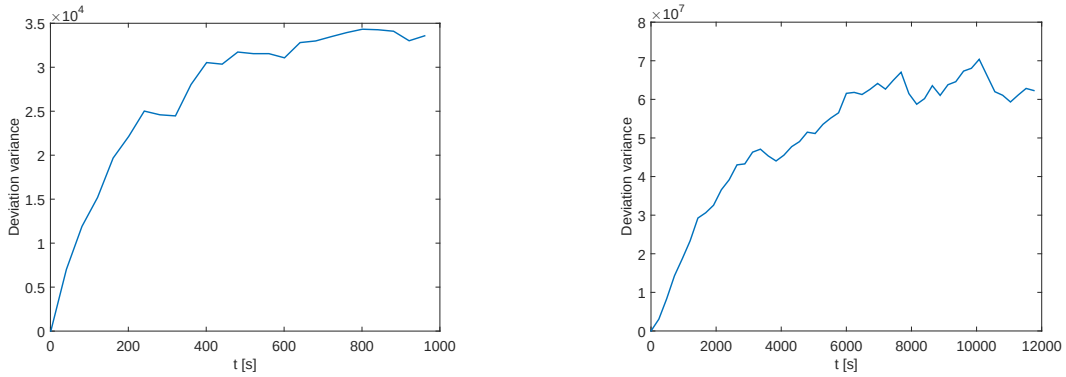

(a) 1-D torus (b) 1-D leader-follower

Figure 21: Deviation from average variance settling time of 80 vehicle 1-D torus and 1-D leader-follower structure.

The prolonged settling may be caused by different communication structure of leader-follower systems, mainly by their double communication graph radius.

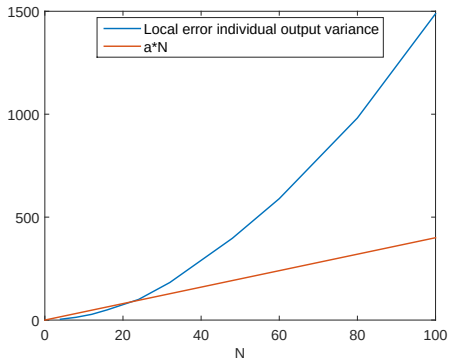

(a) linear axes

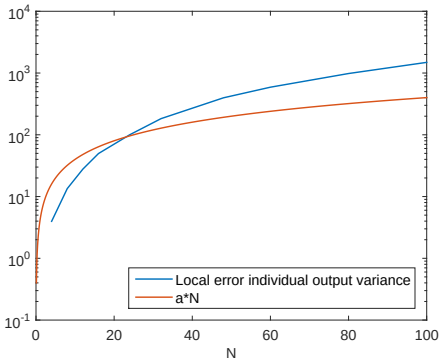

(b) semilog axes

Figure 22: Scaling of local error individual output variance for 1-D leader-follower structure.

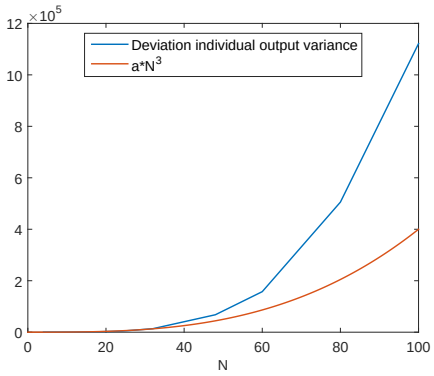

(a) linear axes

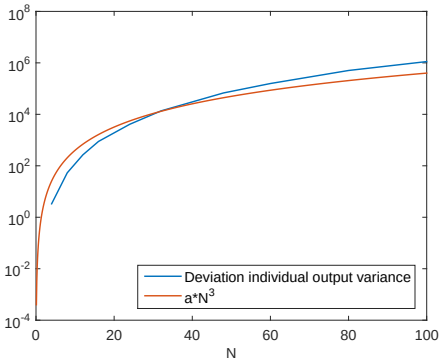

(b) semilog axes

Figure 23: Scaling of deviation from average individual output variance for 1-D leader-follower structure.

Figures 22 and 23 show scaling of variances for 1-D leader-follower structure. Despite the fact that this communication structure is one dimensional, we can see that the type of scaling does not match the scaling for 1-D toroidal structures according to table 1. The reasons for this may be similar to the reasons for longer settling time of the variances. Another reason may be that there is a wave reflection on the rear end of the platoon (reflection on the free-end boundary with the same polarity) [13] that causes variances to scale faster.

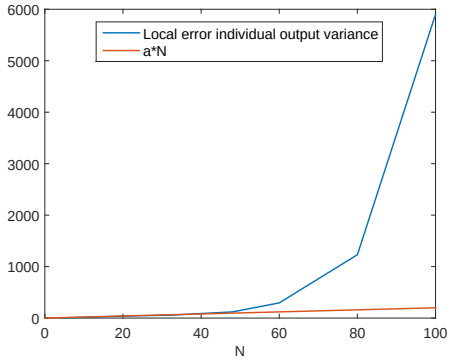

(a) linear axes

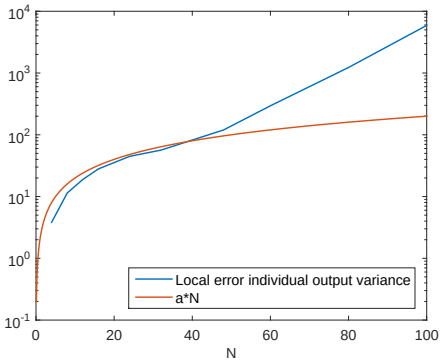

(b) semilog axes

Figure 24: Scaling of local error individual output variance for 1-D leader-follower structure with asymmetric control.

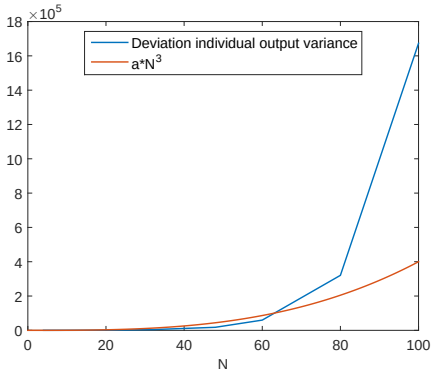

(a) linear axes

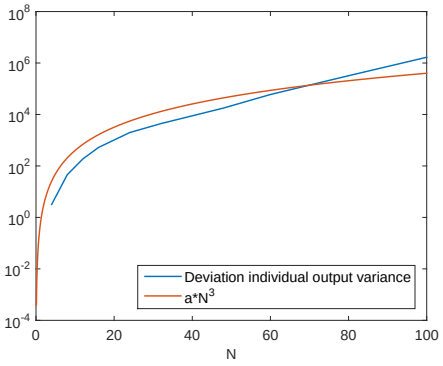

(b) semilog axes

Figure 25: Scaling of deviation from average individual output variance for 1-D leader-follower structure with asymmetric control.

In figures 24 and 25 we can see that system with asymmetric control scales even worse than leader-follower system with symmetric control. Systems with asymmetric control are much more volatile than systems with symmetric control. For systems with asymmetric control certain oberved characteristics scale exponentially with the number of vehicles [12], which may cause worse variance scaling. Graphs in figure 26 show individual output variances (16) for system with asymmetric control fitted with exponential function. We can see, that the type of scaling is indeed exponential.

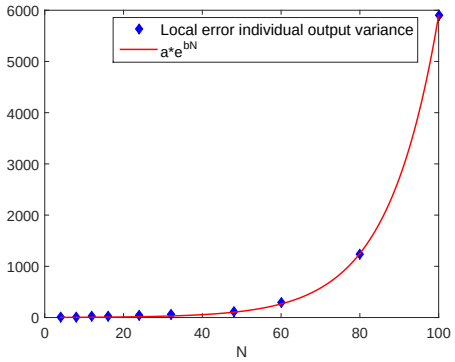

(a) local error
$y = 2.532e^{0.078N}$

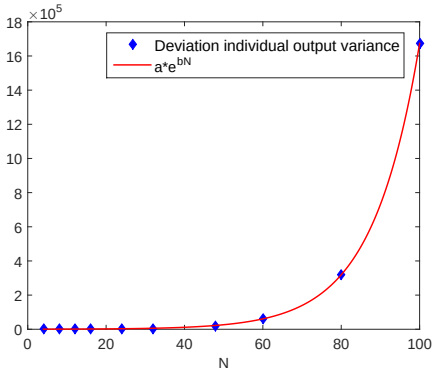

(b) deviation from average
$y = 422e^{0.083N}$

Figure 26: Variances for 1-D leader-follower system with asymmetric control fitted with exponential function $a \cdot e^{bN}$.

3 Linear systems with optimal localized state space control

This chapter focuses on systems with optimal state space control. Our goal is to find an optimal state space controller with control effort comparable to the controller used in previous chapter using LQR criterion.

Then we run the simulations described in chapter 2 on selected system with created optimal controller and compare the results to those from previous chapter. The simulations will be run for two communication structures: 1-D torus and 1-D leader-follower structure, as these two structures had most significant results in previous simulations.

As was already mentioned in chapter 2, using optimally designed controller should not drastically change the behavior of the system (accordion-like motion) nor should it change the type of scaling of the preformance measure variances [2]. That is for selected 1-D toroidal system microscopic measures should still scale linearly and macroscopic measures should have cubic scaling. The difference in the controllers might however change the rate of scaling. We expect that the performance of the optimal controller will be better and the variances will, with increasing number of vehicles, scale slower.

3.1 Linear Quadratic Regulatory (LQR)

Let us consider a system model

$$\dot{x} = Ax + Bu, \qquad t \geq 0 \tag{23}$$

$$\tag{24}$$

The system has infinite-horizon performance index

$$J(0) = \frac{1}{2}\int_0^\infty (x^*Qx + u^*Ru)\, dt \text{ [8]} \tag{25}$$

where $Q \geq 0$ is positive semi-definite matrix, $R > 0$ is positive definite matrix and both Q and R are symmetric. Then for optimal feedback control we get [8]

$$0 = A^*S + SA - SBR^{-1}B^*S + Q \tag{26}$$

$$K = R^{-1}B^*S \tag{27}$$

$$u = -Kx \tag{28}$$

3.2 Controller creation

To design the optimal state space controller, Control System Toolbox function $lqr()$ was used. The function minimalizes system performance index (25).

To ensure the comparability of simulation results in this chapter with those in chapter 2 we compared control efford of these two controllers on system with double integrator.

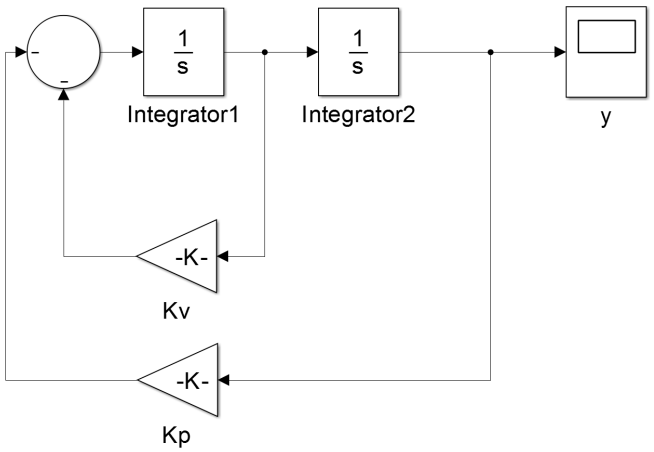

Figure 27: Schema of the system used to compare optimal controller and empirically chosen controller.

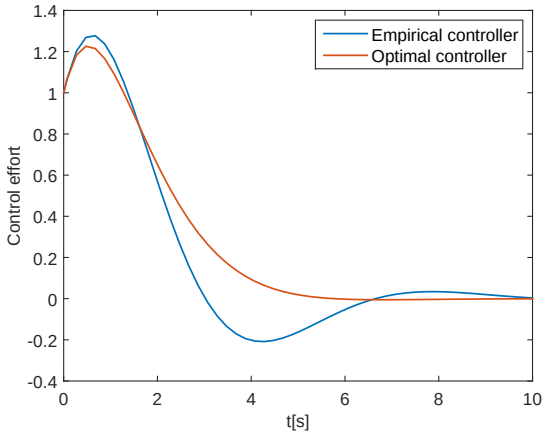

Figure 28: Comparison of the control effort of the optimal controller and empirically chosen controller.

Using the $lqr()$ function we created optimal controller with following gains:

$$k_p = 1.0000 \qquad k_v = 1.7321 \tag{29}$$

From the graph in the figure 28 it is clear that the control effort of the optimal and the suboptimal controller is very similar. Due to this, it should be possible to evaluate the results of the following simulation and compare them to results from chapter 2 without factoring in the difference in control effort of the controllers.

3.3 Inverse optimality

When we designed the optimal regulator for our vehicle model, we first selected the criterion and then we designed the controller accordingly. Inverse optimality works on the opposite

principle. We have designed the controller and we test if it is optimal for a criterion [4].

This can be used in case of localized feedback. In general, if we design an optimal controller for entire network, we obtain centralized feedback [2]. We can however design an optimal controller for one vehicle and then use inverse optimality to see whether there is a criterion for which the controller is optimal in terms of entire network.

Let us have a system

$$\dot{x} = (I_N \otimes A)x + (I_N \otimes B)u. \tag{30}$$

We have the control law

$$u = -c(L \otimes K_2)x \tag{31}$$

where coupling gain $c > 0$, and K_2 represents local feedback matrix. We get global closed loop system.

$$\dot{x} = (I_N \otimes A - cL \otimes BK_2)x \text{ [4]} \tag{32}$$

Following theorem was taken from [4, Theorem 2]:
Consider system

$$\dot{x} = (I_N \otimes A)x + (I_N \otimes B)u. \tag{33}$$

Suppose there are matrices P_1, P_2 where $P_1 = P_1^* \geq 0$ is a positive semi-definite matrix and $P_2 = P_2^* > 0$ is positive definite matrix that satisfy

$$P_1 = cR_1L, \tag{34}$$

$$A^*P_2 + P_2A + Q_2 - P_2BR_2^{-1}B^*P_2 = 0, \tag{35}$$

for some $Q_2 = Q_2^* > 0, R_1 = R_1^* > 0, R_2 = R_2^* > 0$ and a coupling gain $c > 0$. Define the feedback gain matrix K_2 as

$$K_2 = R_2^{-1}B^*P_2 \tag{36}$$

Then the control $u = -cL \otimes K_2x$ is optimal with respect to the performance index

$$J(x_0, u) = \int_0^\infty x^*[c^2(L \otimes K_2)^*(R_1 \otimes R_2)(L \otimes K_2) - cR_1L \otimes (A^*P_2 + P_2A)]x + u^*(R_1 \otimes R_2)u \; dt. \tag{37}$$

$$J(x_0, u) = \int_0^\infty x^*Qx + u^*Ru \; dt. \tag{38}$$

Let us apply the inverse optimality principle on our 1-D toroidal structure of four vehicles. The Laplacian of 1-D toroidal structure has eigenvalues equal to zero. Due to this, we can not stabilize the system. To prevent this problem we add a virtual leader that leads the formation but is not part of it (39).

$$L = \begin{pmatrix} 2 & -1 & 0 & -1 \\ -1 & 2 & -1 & 0 \\ 0 & -1 & 2 & -1 \\ -1 & 0 & -1 & 2 \end{pmatrix} \qquad L_{lead} = \begin{pmatrix} 3 & -1 & 0 & -1 \\ -1 & 2 & -1 & 0 \\ 0 & -1 & 2 & -1 \\ -1 & 0 & -1 & 2 \end{pmatrix} \tag{39}$$

This ensures that laplacian has only positive eigenvalues. The laplacian is symmetric, which means we can choose $c = 1$ and $R_1 = I_N$. K_2 was previously determined as $K_2 = [1.0000 \quad 1.7321]$. Matrices Q_2, R_2 are the same we used with $lqr()$ to determine the feedback gain matrix K_2 and matrix P_2 is one of the outputs of $lqr()$ function. We have everything needed to determine the performance index (37).

$$Q = \begin{pmatrix} 33.0 & 41.6 & -15.0 & -20.8 & 6.0 & 10.4 & -15.0 & -20.8 \\ 41.6 & 81.0 & -20.8 & -39.0 & 10.4 & 18.0 & -20.8 & -39.0 \\ -15 & -20.8 & 18.0 & 20.8 & -12.0 & -15.6 & 6.0 & 10.4 \\ -20.8 & -39.0 & 20.8 & 42.0 & -15.6 & -30.0 & 10.4 & 18.0 \\ 6.0 & 10.4 & -12.0 & -15.6 & 18.0 & 20.8 & -12.0 & -15.6 \\ 10.4 & 18.0 & -15.6 & -30.0 & 20.8 & 42.0 & -15.6 & -30.0 \\ -15.0 & -20.8 & 6.0 & 10.4 & -12.0 & -15.6 & 18.0 & 20.8 \\ -20.8 & -39.0 & 10.4 & 18.0 & -15.6 & -30.0 & 20.8 & 42.0 \end{pmatrix} \quad R = \begin{pmatrix} 3 & 0 & 0 & 0 \\ 0 & 3 & 0 & 0 \\ 0 & 0 & 3 & 0 \\ 0 & 0 & 0 & 3 \end{pmatrix} \tag{40}$$

Now we can use the $lqr()$ function with our performance index (40) on the entire network. We recieve the feedback gain matrix K for the network that equals to $L \otimes K_2$ (41), (42), which confirms the optimality of the designed feedback controller.

$$K = \begin{pmatrix} 3.000 & 5.196 & -1.000 & -1.732 & 0.000 & 0.000 & -1.000 & -1.732 \\ -1.000 & -1.732 & 2.000 & 3.464 & -1.000 & -1.732 & 0.000 & 0.000 \\ 0.000 & 0.000 & -1.000 & -1.732 & 2.000 & 3.464 & -1.000 & -1.732 \\ -1.000 & -1.732 & 0.000 & 0.000 & -1.000 & -1.732 & 2.000 & 3.464 \end{pmatrix} \tag{41}$$

$$(L_{lead} \otimes K_2) = \begin{pmatrix} 3.000 & 5.196 & -1.000 & -1.732 & 0.000 & 0.000 & -1.000 & -1.732 \\ -1.000 & -1.732 & 2.000 & 3.464 & -1.000 & -1.732 & 0.000 & 0.000 \\ 0.000 & 0.000 & -1.000 & -1.732 & 2.000 & 3.464 & -1.000 & -1.732 \\ -1.000 & -1.732 & 0.000 & 0.000 & -1.000 & -1.732 & 2.000 & 3.464 \end{pmatrix} \tag{42}$$

Equation (40) shows the criterion for our optimal localized feedback. As we can see from the Q matrix, this criterion is very unintuitive. Usually, to design feedback, one would use diagonal criterion. However, obtained matrix Q is not diagonal. In fact it has all elements nonzero. This means that the criterion penalizes even products of states that are not othervise related in terms of the network.

3.4 Vehicle trajectory simulation

We run the vehicle trajectory simulation described in chapter 2.2 for selected systems with newly created optlimal state space controller to see, whether the change of the controller significantly alters system behavior in terms of relative vehicle position.

3.4.1 Results of the simulation

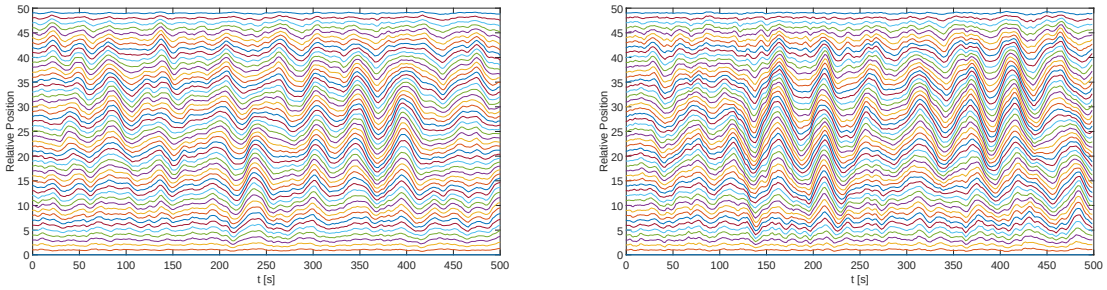

(a) optimal control (b) suboptimal control

Figure 29: Comparison of vehicle position trajectories of a 50 vehicle 1-D torus with optimal and suboptimal control.

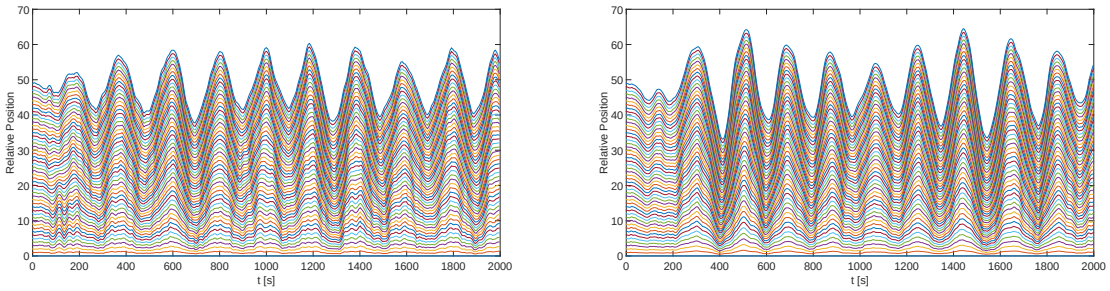

(a) optimal control (b) suboptimal control

Figure 30: Comparison of vehicle position trajectories of a 50 vehicle 1-D leader-follower structure with optimal and suboptimal control.

The figures 29 and 30 show that using optimal controller does not change the results of our simulation on large scale. This is an expected result as the accordion-like motion should manifest in all systems representing large formations with only localized feedback [2].

3.5 Comparison between system with optimal and suboptimal control

Similarly to the previous subchapter, here we run the simulation used to verify scaling of the performance measure (17), (18) individual output variances (16) described in chapter 2.6

on selected systems with optimal controller.

The results of the simulation are compared with the results from chapter 2. This way it is possible to determine whether our assumptions from the begining of the chapter were correct or not.

3.5.1 Results of the simulation

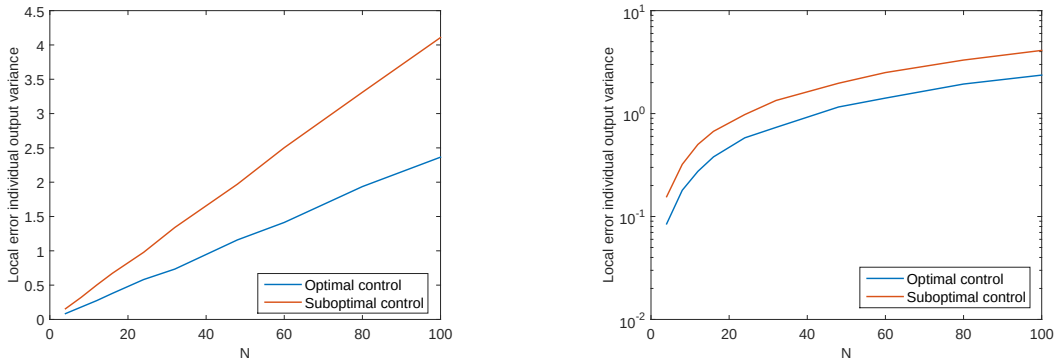

(a) linear axes (b) semilog axes

Figure 31: Comparison of the scaling of local error individual output variance for 1-D torus with optimal and suboptimal control.

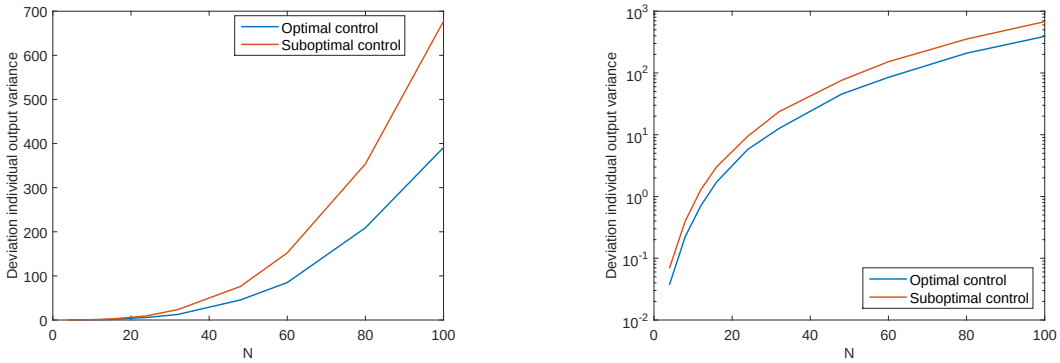

(a) linear axes (b) semilog axes

Figure 32: Comparison of the scaling of deviation from average individual output variance for 1-D torus with optimal and suboptimal control.

Figures 31 and 32 show the difference in scaling of the 1-D toroidal systems with optimal and suboptimal state space control.

Firstly, we see whether the types of scaling in the graphs in figures 31 and 32 correspond to those stated in table 1. It is clear from the graphs, that the type of scaling has not changed by adding optimal controller. This is consistent with [2].

Secondly, we want to verify our assumption that scaling will be slower with the optimal controller. From the graphs above it is clear that while type of scaling remains the same, linear for local error and cubic for deviation from average, systems with optimal controller scale with number of vehicles at lower rate than system with suboptimal state space control.

While the decrease in scaling rate is noticable, it is not significant enough to considerably affect the overall behavior of the system. This was alreary shown in previous experiment (see chapter 3.4).

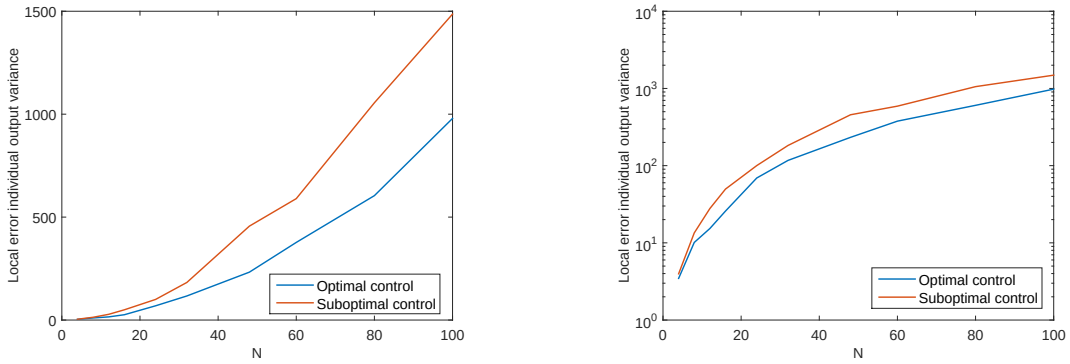

(a) linear axes (b) semilog axes

Figure 33: Comparison of the scaling of local error individual output variance for 1-D leader-follower structure with optimal and suboptimal control.

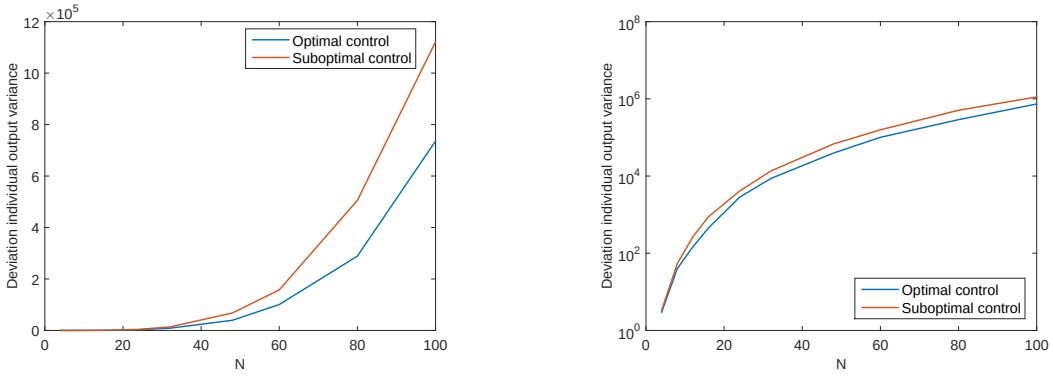

(a) linear axes (b) semilog axes

Figure 34: Comparison of the scaling of deviation from average individual output variance for 1-D leader-follower structure with optimal and suboptimal control.

Figures 33 and 34 show the difference in scaling of the 1-D leader-follower systems with optimal and suboptimal state space control.

It is clear that despite the fact that the variances of leader-follower systems do not scale according to our initial assumption, using optimal state space controller lowers the scaling rate of the variances similarly to those of 1-D torus.

4 Systems with static nonlinearities

While chapters 2 and 3 focused on linear systems, in this chapter we study systems nonlinear. Similarly to the previous chapter the simulations will be run on 1-D toroidal communication structure and on 1-D leader-follower structure.

Our goal is to evaluate the effect of static nonlinearities (we will focus on saturation) on the behavior of the system and scaling of the variances from chapter 2.3.

Simulated systems are subjected to random disturbances. These disturbances will be affected by the saturation. Our assumption is that the saturation may diminish the effects of these disturbances and the performance measure variances might scale at slower rate. The type of scaling should however remain the same [2] as the nature of the system is not changed.

4.1 System Description

For the purpose of simulations in this chapter we used system described in figure 2 and added saturation.

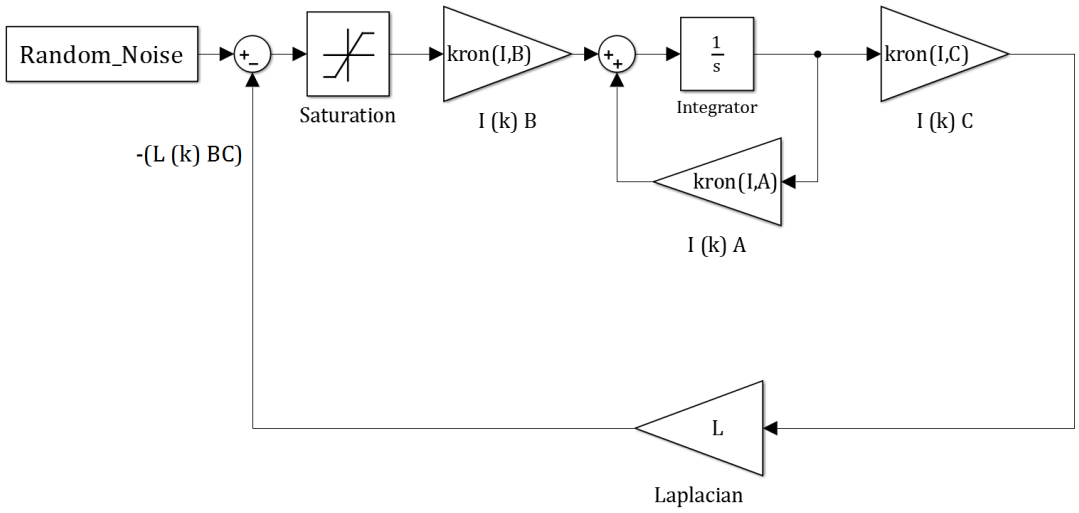

Figure 35: Block schema of the system with added saturation.

To determine the bounds of saturation we used the leader-follower communication structure. We removed random disturbances and changed the initial condition for leader velocity from zero to nonzero value. We run vehicle trajectory simulation and observed control effort for individual vehicles in time.

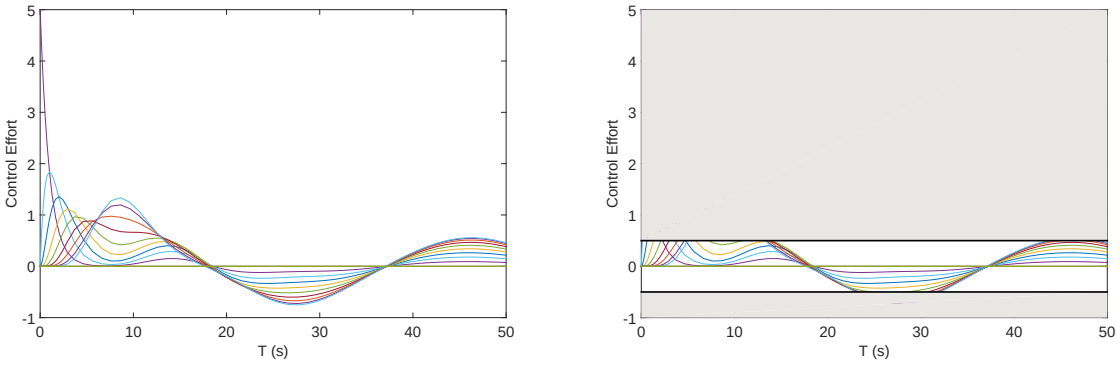

(a) control effort (b) saturation bounds

Figure 36: Saturation bounds selection - control effort of the 1-D leader-follower communication structure.

The saturation bounds value was determined so that it affects the states during the entire simulation and not only for the first spike (see figure 36). In line with previous statement we chose the saturation bounds as ± 0.5.

4.2 Vehicle trajectory simulation

The goal of this simulation is to compare the behavior of system with added saturation to that of system without saturation.

4.2.1 Results of the simulation

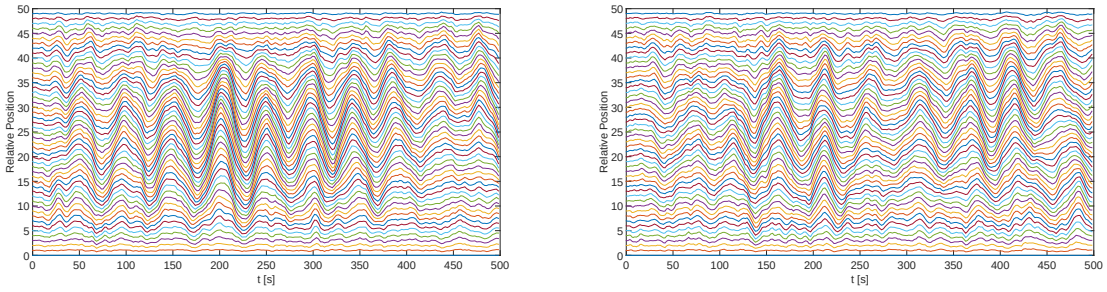

(a) saturation (b) no saturation

Figure 37: Comparison of vehicle position trajectories of a 50 vehicle 1-D torus with and without saturation.

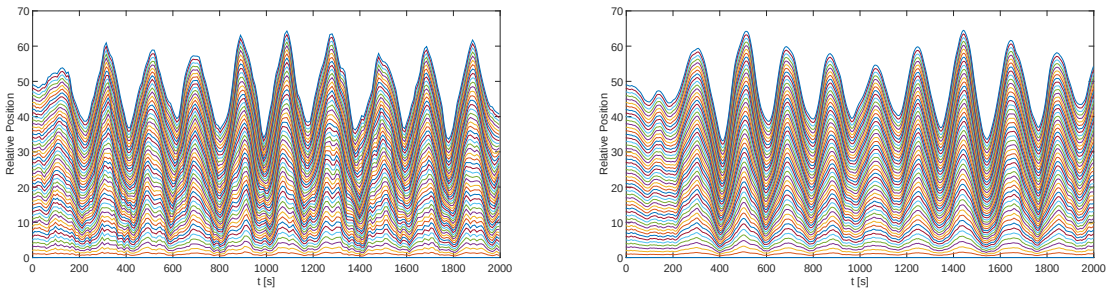

(a) saturation (b) no saturation

Figure 38: Comparison of vehicle position trajectories of a 50 vehicle 1-D leader-follower structure with and without saturation.

From figures 37 and 38 it is clear that systems with saturation still retain the accordion-like behavior of systems without saturation.

4.3 Comparison between system with and without static nonlinearities

This simulation is focused on the effect of added saturation on scaling of performance measure (17), (18) individual output variances (16). Variances of systems with saturation are compared to those of systems without saturation.

4.3.1 Results of the simulation

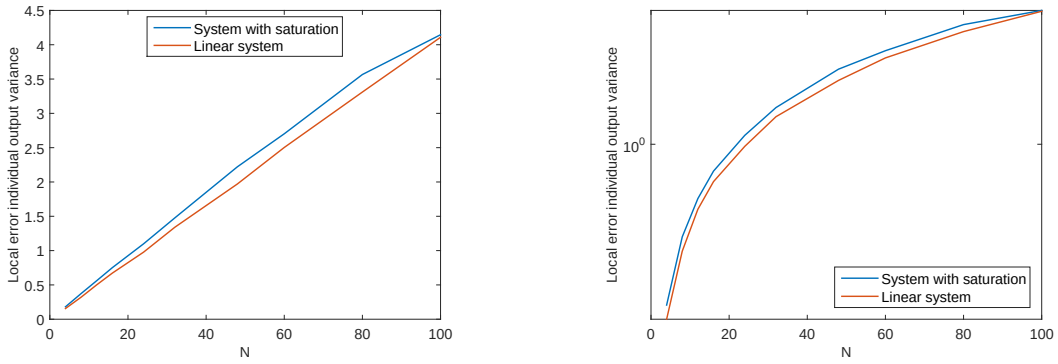

(a) linear axes (b) semilog axes

Figure 39: Comparison of the scaling of local error individual output variance for 1-D torus with and without saturation.

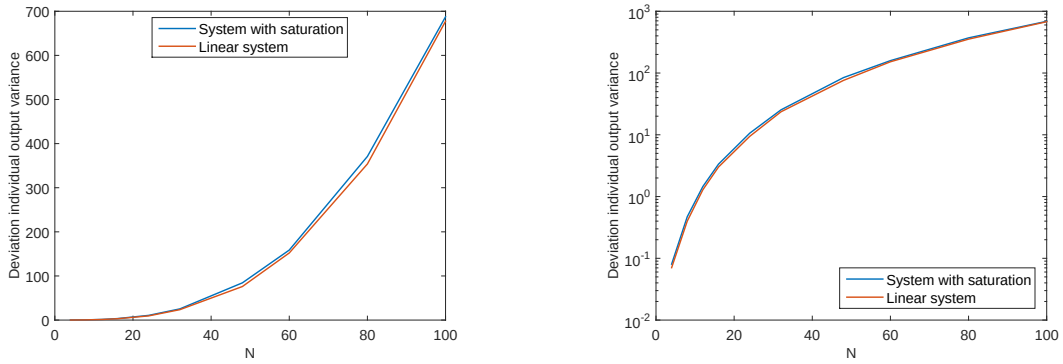

(a) linear axes (b) semilog axes

Figure 40: Comparison of the scaling of deviation from average individual output variance for 1-D torus with and without saturation.

Figures 39 and 40 depict the scaling of performance measure variances for 1-D torus with and without saturation.

The original assumption was that saturation will diminish the scaling rate of the variances. This is clearly not the case. In fact variances of system with saturation scale slightly faster than those of system without saturation. The explanation for this can be that while saturation affects random disturbances it also limits the control effort and therefore diminishes the effect of the controller on the behavior of the system.

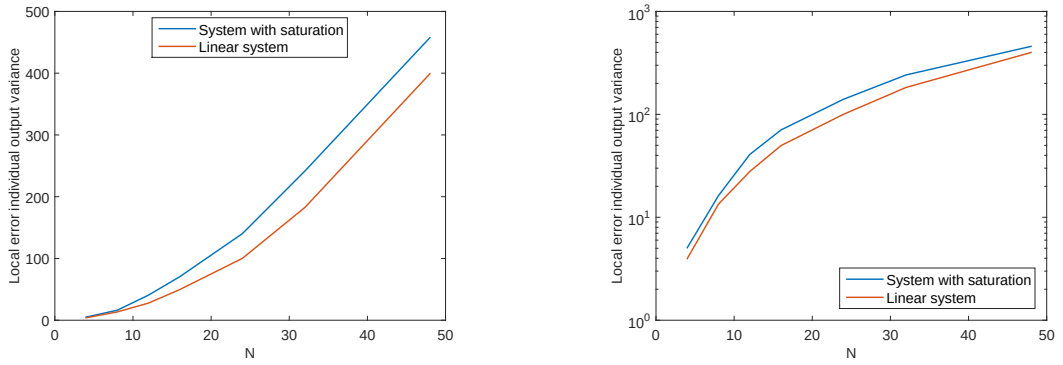

(a) linear axes (b) semilog axes

Figure 41: Comparison of the scaling of local error individual output variance for 1-D leader-follower structure with and without saturation.

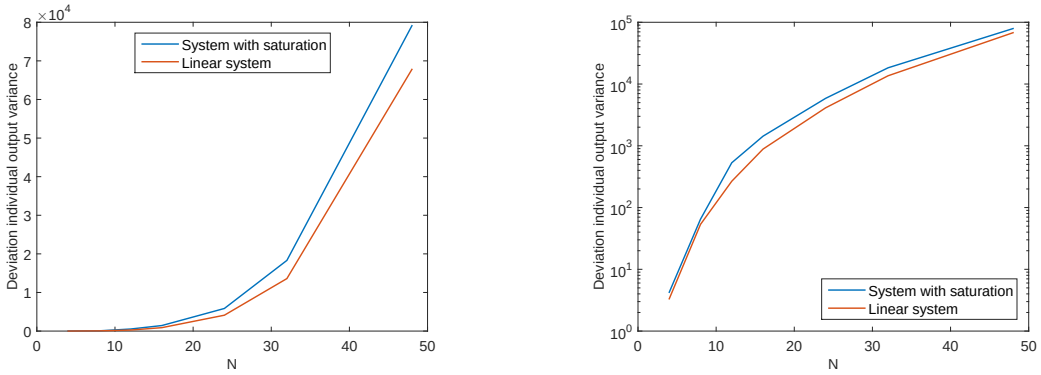

(a) linear axes

(b) semilog axes

Figure 42: Comparison of the scaling of deviation from average individual output variance for 1-D leader-follower structure with and without saturation.

The performance measure variances for 1-D leader-follower structure are shown in the figures 41 and 42.

It is important to note that the amount of time as well as computing power required to run the simulations for systems with saturation was several times higher than for systems without saturation. This together with very long settling time for variances of leader-follower systems mentioned in chapter 2 meant that we were only able to run the simulation for counts of vehicles up to 50. This should not however affect the result of the simulation.

In the figures 41 and 42 we can see that the results for 1-D leader-follower are similar to those of 1-D torus. The explanation for faster scaling rate of system with saturation will therefore be the same.

5 Second order system with PI controller

In previous chapters we studied the behavior of the systems with state space model described in (6) and (7) with either different type of state space controller or saturation. In this chapter we created system with different state space model.

5.1 System description

The state space model:

$$\dot{\mathbf{x}} = A\mathbf{x} + B\mathbf{u} \tag{43}$$

$$\dot{\mathbf{y}} = C\mathbf{x} \tag{44}$$

$$A = \begin{pmatrix} 0 & 1 \\ 0 & -a \end{pmatrix} \qquad B = \begin{pmatrix} 0 \\ 1 \end{pmatrix} \tag{45}$$

$$C = \begin{pmatrix} k_p & k_v \end{pmatrix} \qquad D = \begin{pmatrix} 0 \end{pmatrix} \tag{46}$$

For the purpose of our simulations we chose the feedback gains $k_p = 1$ and $k_v = 1$, same as in chapter 2.

The state space model represents a vehicle similar to those from chapter 2 to which we added resistance in the form of coefficient $-a$. To this system we added a PI controller. By adding the PI controller we ensure that our system has the characteristics of system with double integrator similarly to systems in previous chapters.

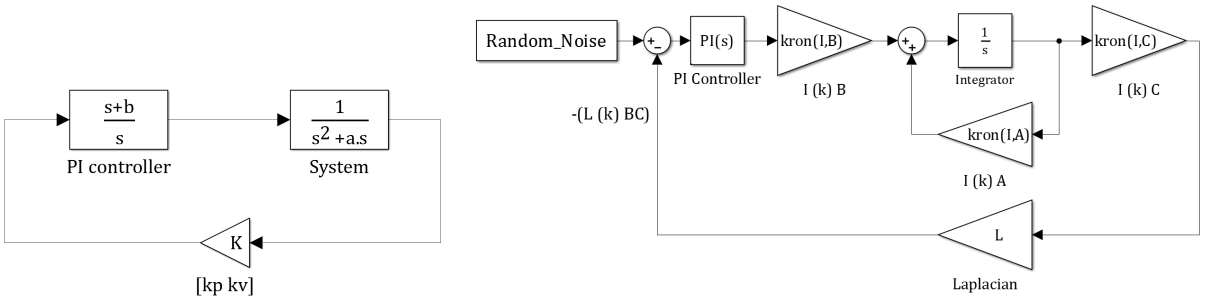

(a) vehicle model (b) entire system

Figure 43: Vehicle model and system block representation.

The vehicle model system with PI controller has two poles in 0. One originates from the system itself and one is part of the controller. This secures the double integrator character. Due to the added resistance, there is another pole in $-a$ and the PI regulator adds zero in $-b$. To ensure stability we need to make sure that $b < a$. For our purposes we have chosen $b = 2,\ a = 4$.

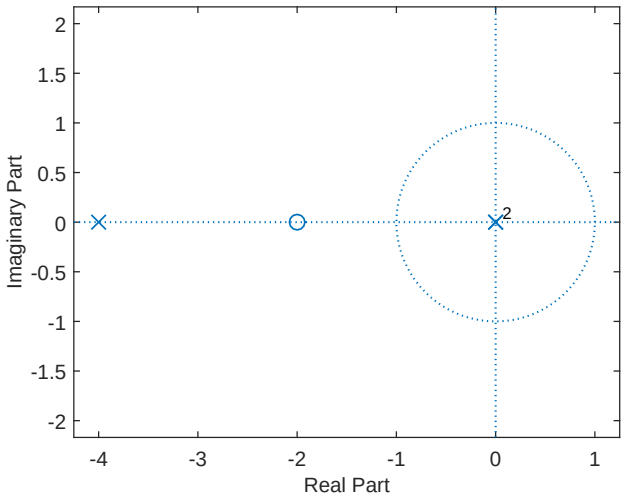

Figure 44: Zero-pole diagram of the system.

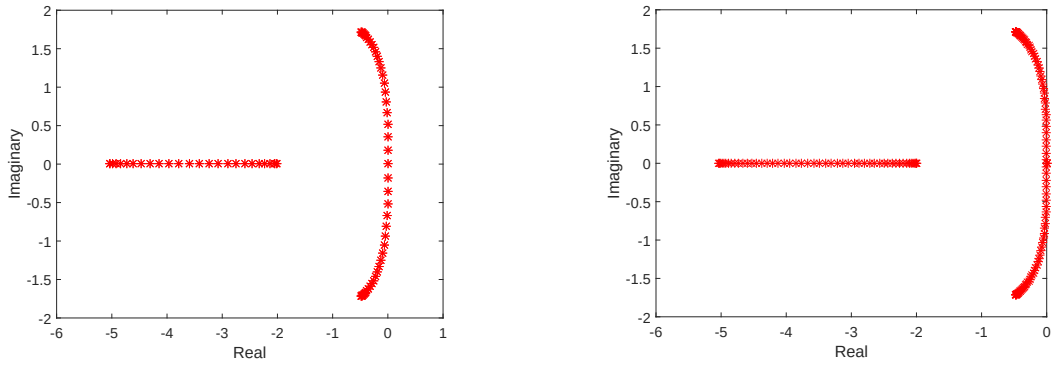

(a) 1-D torus

(b) 1-D leader-follower

Figure 45: Eigenvalues of system with resistance and PI controller with 1-D torus structure and 1-D leader-follower structure.

Figure 45 shows eigenvalues of systems studied in this chapter. For both 1-D torus and 1-D leader-follower structure eigenvalues lie in the left half-plane of the complex plane. This ensures the stability of the systems.

This series of simulations is motivated by assumption that, espetially for high vehicle counts N, the influence of the nonzero pole will be negligible, that is, the behavior of the systems will be comparable to that of systems from chapter 2.

Similarly to chapters 3 and 4, all simulations will be performed on 1-D toroidal structure and 1-D leader-follower structure.

5.2 Vehicle trajectory simulation

Despite the differences of system studied in this chapter to those from previous chapters, we belive that overall behavior of the system will be the same. That is, it will be possible to observe the accordion motion in the results of the vehicle trajectory simulation of the platoon.

5.2.1 Results of the simulation

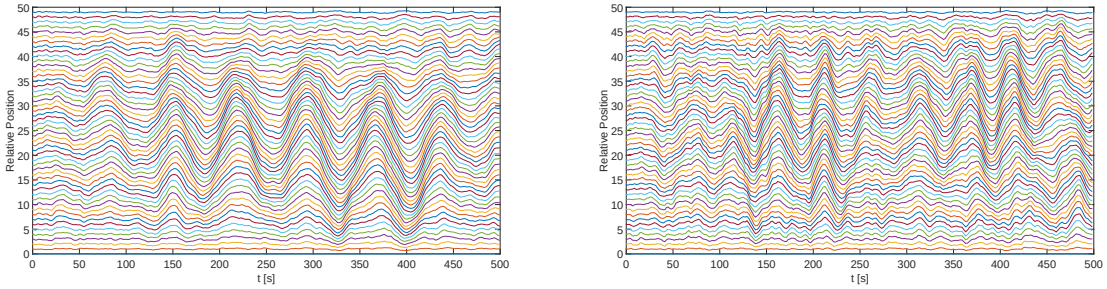

(a) system with resistance and PI controller (b) double integrator

Figure 46: Comparison of vehicle position trajectories of a 50 vehicle 1-D torus for system with resistance and PI controller and double integrator system.

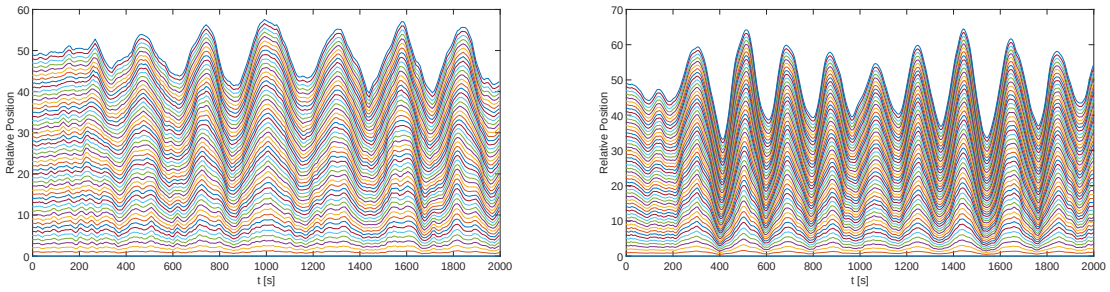

(a) system with resistance and PI controller (b) double integrator

Figure 47: Comparison of vehicle position trajectories of a 50 vehicle 1-D leader-follower structure for system with resistance and PI controller and double integrator system.

In both figures 46 and 47 we can see that systems with resistance and PI controller retained the accordion-like behavior of the double integrator systems from chapter 2. This confirms the assumption that the characteristics of double integrator contained in the systems outweigh the influence of nonzero pole of the system.

5.3 Comparison between system with resistance and PI controller and double integrator

In line with assumptions and results presented above, we expect systems with resistance and PI controller to have the same type of performance measure (17), (18) individual output variance (16) scaling as respective double integrator systems.

5.3.1 Results of the simulation

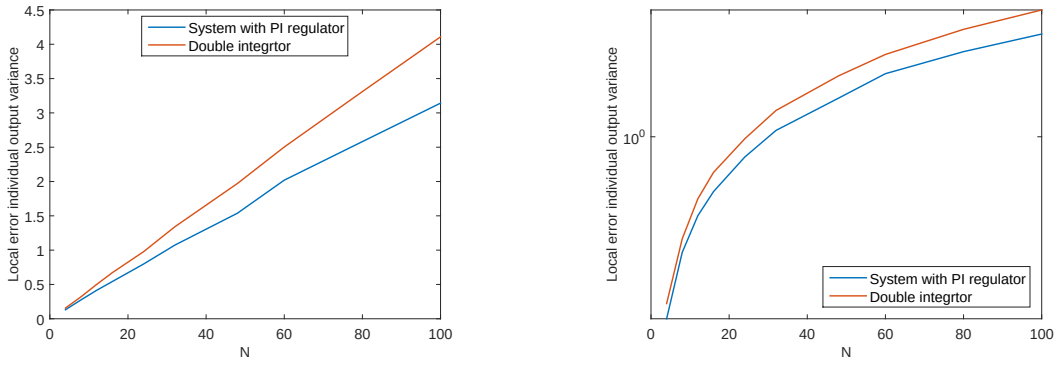

(a) linear axes (b) semilog axes

Figure 48: Comparison of the scaling of local error individual output variance for 1-D torus system with resistance and PI controller and double integrator system.

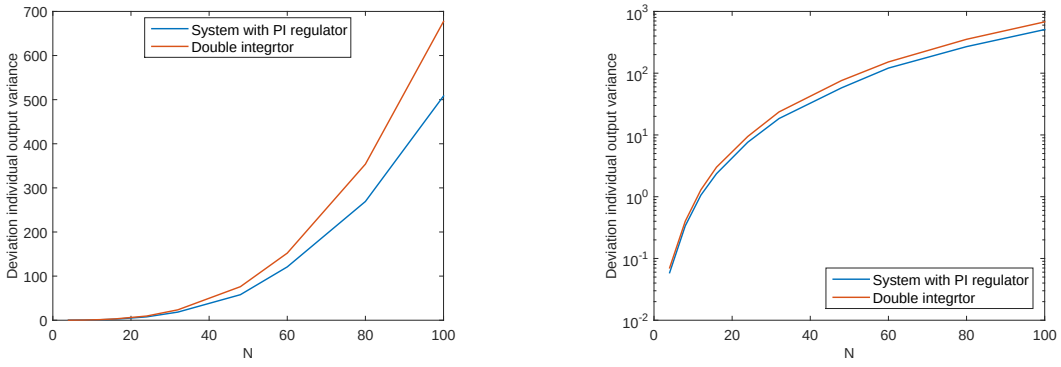

(a) linear axes (b) semilog axes

Figure 49: Comparison of the scaling of deviation from average individual output variance for 1-D torus system with resistance and PI controller and double integrator system.

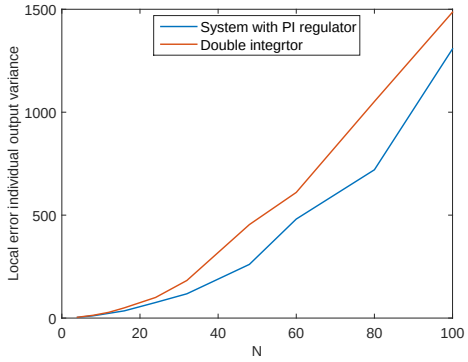

(a) linear axes

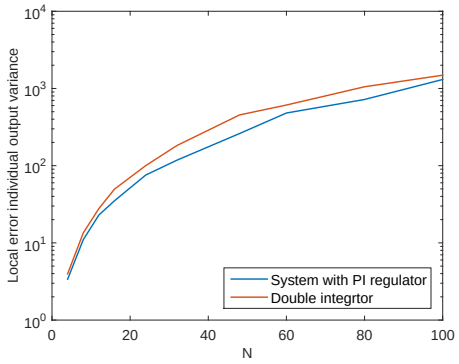

(b) semilog axes

Figure 50: Comparison of the scaling of local error individual output variance for 1-D leader-follower system with resistance and PI controller and double integrator system.

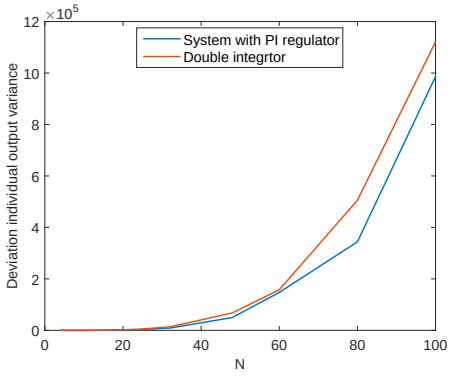

(a) linear axes

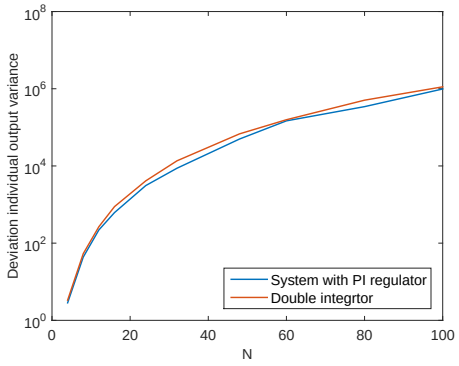

(b) semilog axes

Figure 51: Comparison of the scaling of deviation from average individual output variance for 1-D leader-follower system with resistance and PI controller and double integrator system.

Figures 48 and 49 show scaling of variances of 1-D torus structures, figures 50 and 51 show scaling of variances of 1-D leader-follower structures.

From the graphs it is clear that, while the systems with resistance scale at a lower rate, the type of scaling is the same. This is true for both 1-D torus and 1-D leader-follower structure.

The results support our theory that the double integrator in the system has much larger impact on its overall behavior than the nonzero pole.

6 Conclusion

The theoretical part of the thesis was focused on desriptions of simulated systems. The state space model was described as well as various communication structures that were later implemented in Matlab enviroment. Theoretical findings, necessary to understand the motivation of the simulations performed in the thesis, were presented. There were three types of slimulations performed: Vehicle trajectory simulation, Performance measures simulation and Scaling verification.

It is clear from the results of the simulations for 1-D, 2-D and 3-D communication structures, that the more dimensional the structure is the less pronounced is the accordion like motion (the effect of the random disturbances on the formation) [2]. The results verify the type of output variance scaling for 1-D, 2-D and 3-D toroidal structures from [2]. Simulations for 1-D leader-follower structures show that these sctructures are more affected by random disturbances than toroidal structure of the same dimension.

Systems with optimal state space control were compared to those with suboptimal state space control. Optimal control slightly diminishes the influence of random disturbances. However, qualitatively results remain the same.

Saturation was added to the 1-D torus and 1-D leader-follower systems and its influance on system behavior was studied. The addition of saturation only slightly increases the scaling rate of the output variances of the systems.

We introduced new type of system representing vehicle with resistance controlled by PI controller. Simulations for this type of system verify the assumption that characteristics of the system, resulting from it containing two integrators, outweigh the influance of nonzero pole.

This thesis satisfies first three tasks from the bachelor project assignment. After the agreement with thesis supervisor the fourth task, the local Model Predictive Control, was changed and the part studying second order system with PI controller was added instead.

I belive that the simulation results in this thesis provide useful data in the field of local feedback control of large networked systems. The results in this thesis can be expanded in several directions. Firstly, the fact that leader-follower system variances do not scale the same way as variances of systems with toroidal structure is worth following upon. Additionally, studying the scaling of other types of systems or systems with different communication structure might bare valuable results.

7 Bibliography

[1] Safe road trains for the environment project. http://www.sartre-project.eu/, 2009.

[2] B. Bamieh, M. R. Jovanović, P. Mitra, and S. Patterson. Coherence in large-scale networks: Dimension-dependent limitations of local feedback. *Autom. Control. IEEE Trans.*, vol. 57(no. 9):pp. 2235–2249, 2012.

[3] R. D'Andrea and G. Dullerud. Distributed control design for spatially interconnected systems. *Automatic Control. IEEE Trans.*, vol. 48(no. 9):pp. 1478–1495, 2003.

[4] K. Hengster-Movric and F. Lewis. Cooperative optimal control for multi-agent systems on directed graph topologies. *Autom. Control. IEEE Trans.*, vol. 56(no. 3):pp. 769–774, Mar.2014.

[5] I. Herman, D. Martinec, Z. Hurák, and M. Sebek. Nonzero bound on fiedler eigenvalue causes exponential growth of h-infinity norm of vehicular platoon. *Autom. Control. IEEE Trans.*, vol. PP(no. 99):pp. 1–7, 2014.

[6] Roger A. Horn and Charles R. Johnson. *Matrix Analysis*. Cambridge University Press, 1990.

[7] Andrew Knyazev. Laplacian in 1d, 2d, or 3d. http://www.mathworks.com/matlabcentral/fileexchange/27279-laplacian-in-1d–2d–or-3d, 2010.

[8] F. L. Lewis and V. L. Syrmos. *Optimal Control*. John Wiley and Sons, inc., 1995.

[9] F. L. Lewis, H. Zhang, K. Hengster-Movric, and A. Das. *Cooperative Control of Multi-Agent Systems*. Springer, 2014.

[10] D. Martinec, I. Herman, Z. Hurák, and M. Šebek. Wave-absorbing vehicular platoon controller. *Eur. J. Control*, vol. 20:pp. 234–248, 2014.

[11] Dan Martinec. *Distributed control of platoons of racing slot cars*. Czech Technical University in Prague, 2012.

[12] F. Tangerman, J. Veerman, and B. Stosic. Asymmetric decentralized flocks. *Autom. Control. IEEE Trans.*, vol. 57(no. 11):pp. 2844–2853, 2012.

[13] Berkeley University of California. California partners for advanced transportation technology. http://www.path.berkeley.edu/, 1986.

[14] K. Zhou and J. C. Doyle. *Essentials of robust control*. Prentice Hall, 1998.

Appendix A CD Content

Names and contents of all root directories are listed in table 2

Directory name	Description
pdf	this thesis in pdf format.
sources	latex source code
figures	matlab figures containing results of the simulations
scripts	matlab scripts created during the course of this thesis

Table 2: CD Content

Folders figures and scripts contain subfolders corresponding with different simulations. For scripts, in each subfolder there is one script that is fully commented for better understanding of the simulation, other scripts contain only basic commentary. For more information see readme.txt included on the CD.

Appendix B Additional performance measure simulations

Following figures show the comparison between performance measure (17), (18), (19) variances (15) obtained via simulation and variances computed from H_2 norm (20) for 2-D and 3-D torus.

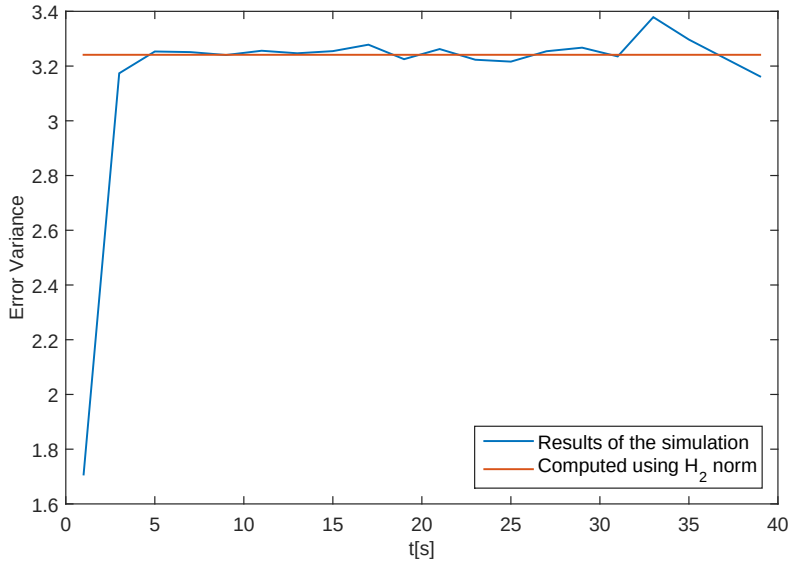

Figure 52: Comparison between local error variance of 2D torus obtained via simulation and variance computed from H_2 norm.

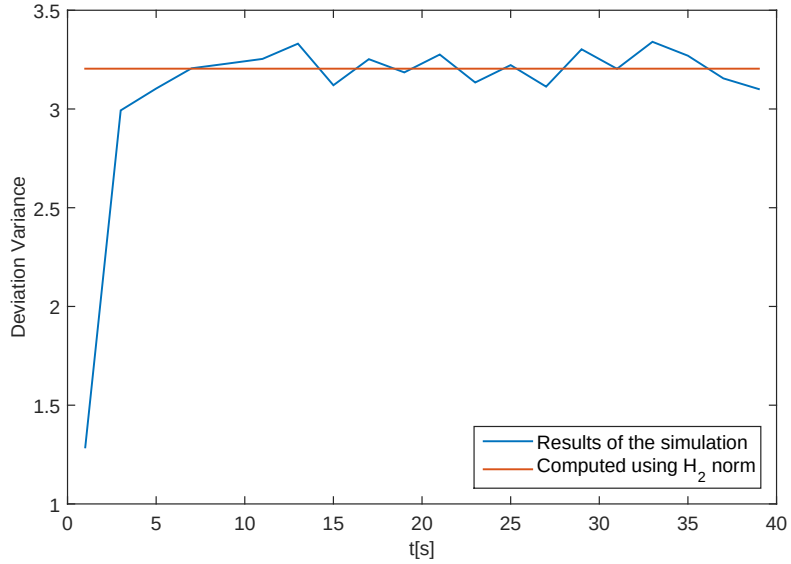

Figure 53: Comparison between deviation from average variance of 2D torus obtained via simulation and variance computed from H_2 norm.

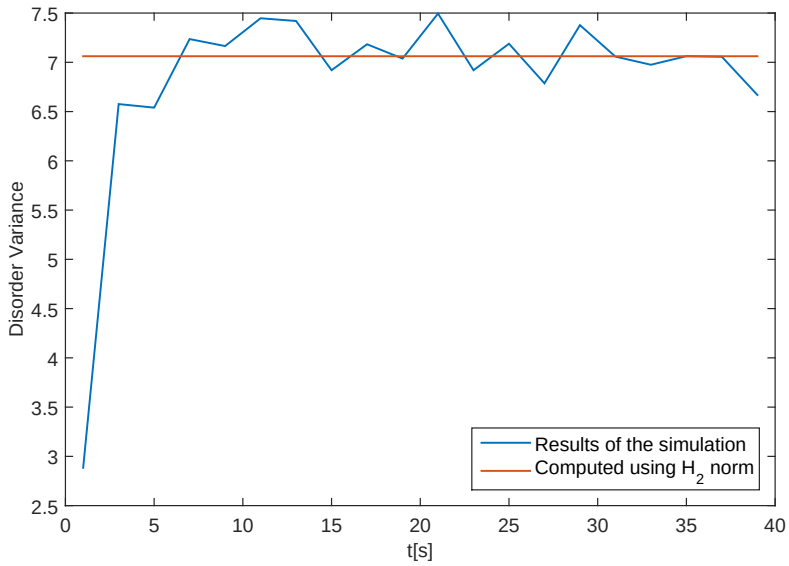

Figure 54: Comparison between disorder variance of 2D torus obtained via simulation and variance computed from H_2 norm.

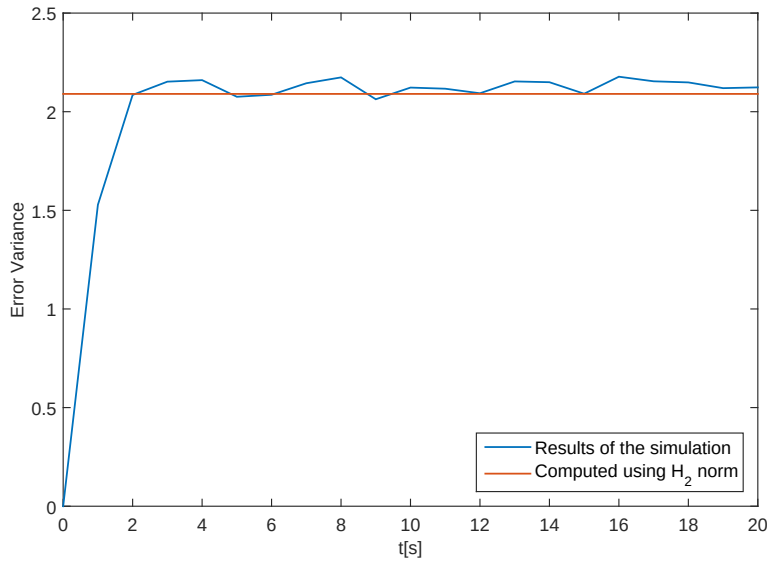

Figure 55: Comparison between local error variance of 3D torus obtained via simulation and variance computed from H_2 norm.

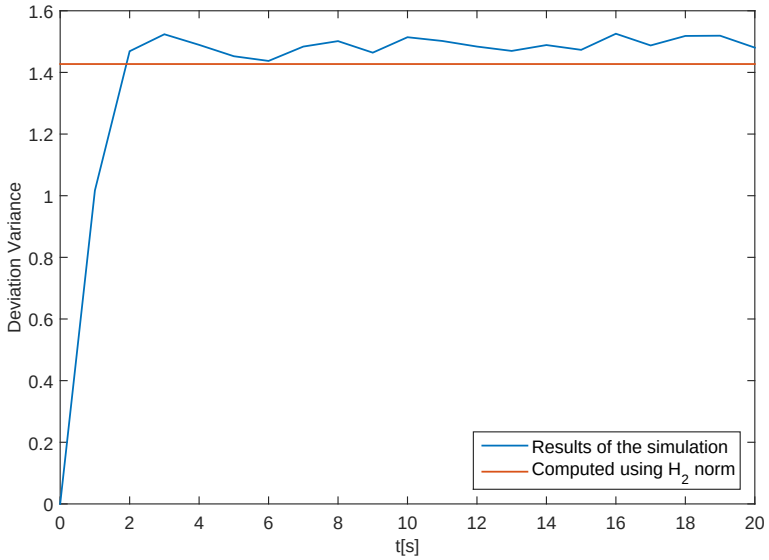

Figure 56: Comparison between deviation from average variance of 3D torus obtained via simulation and variance computed from H_2 norm.

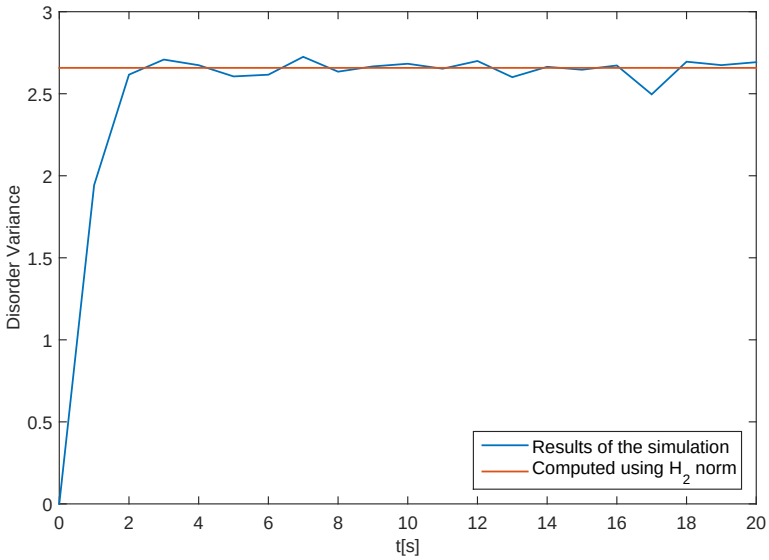

Figure 57: Comparison between disorder variance of 3D torus obtained via simulation and variance computed from H_2 norm.

Appendix C Scaling of disorder for additional systems

Following figures show scaling of disorder (19) individual output variance (16) for various systems.

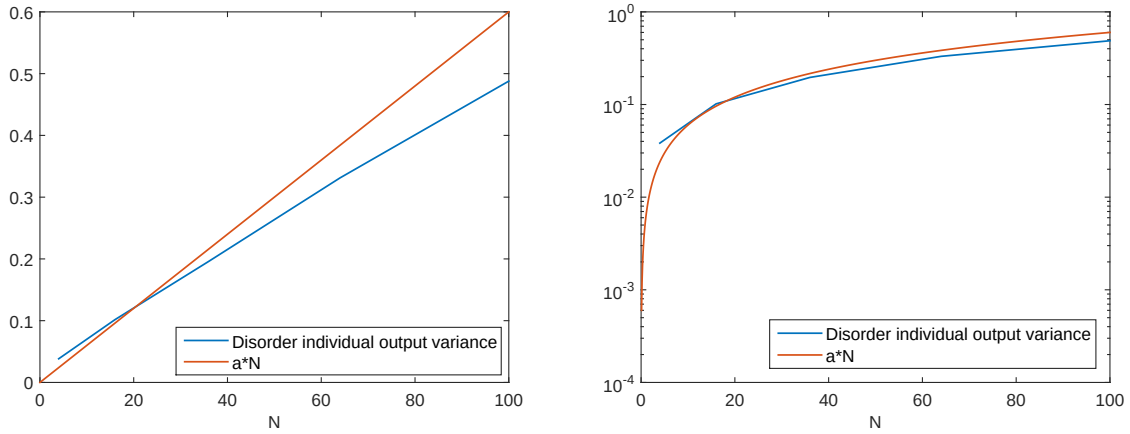

(a) linear axes (b) semilog axes

Figure 58: Scaling of disorder individual output variance for 2-D torus.

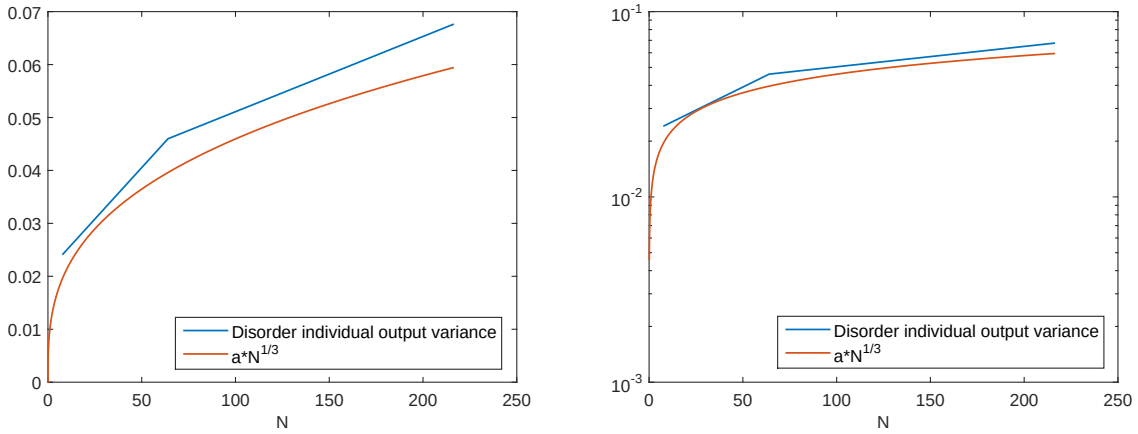

(a) linear axes (b) semilog axes

Figure 59: Scaling of disorder individual output variance for 3-D torus.

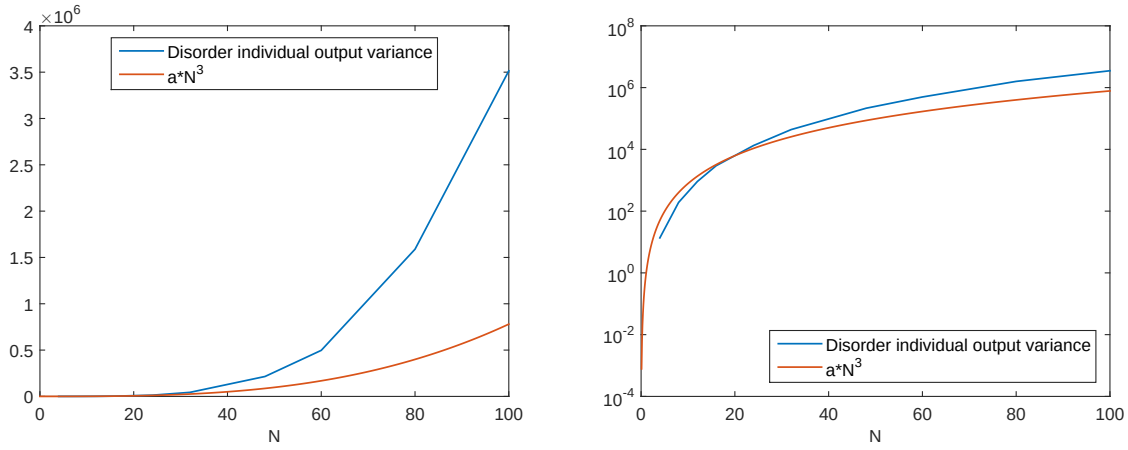

(a) linear axes (b) semilog axes

Figure 60: Scaling of disorder individual output variance for 1-D leader-follower structure.

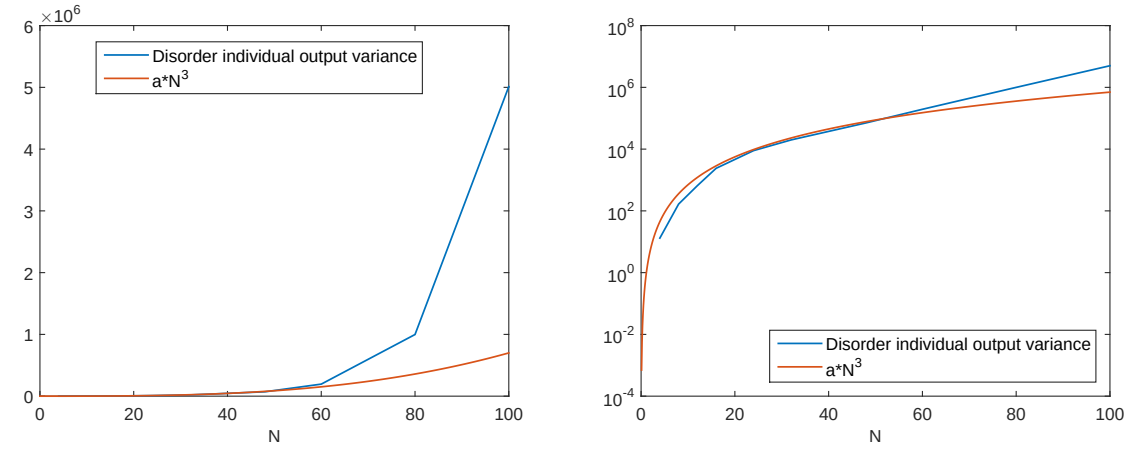

(a) linear axes (b) semilog axes

Figure 61: Scaling of disorder individual output variance for 1-D leader-follower structure with asymmetric control.